Improvement and In-situ Study of Lithium Sulfur Batteries

Master of Science thesis report

By

Q.Liu

4423569

Master of Science

in Sustainable Energy Technology

Materials for Energy Conversion and Storage

Department of Chemical Engineering

Faculty of Applied Science

Delft University of Technology

Supervisor:	Prof. Dr. Ir. F. M. Mulder	
Thesis committee:	Prof. Dr. Ir. F. M. Mulder	TU Delft
	Dr.ir. Marnix Wagemaker	TU Delft
	Dr. Erik Kelder	TU Delft
Daily supervisor:	P. P. R. M. L. Harks MSc	TU Delft

TU Delft Delft University of Technology

TU Delft Delft University of Technology

Challenge the future

Acknowledgement

Since the summer in 2015, I have spent my time on studying and working on Li-S batteries in the MECS group at Reactor Institute Delft. After two years, I have put a great effort into the thesis experiments and finally it has come to the end. Just my curiosity on batteries would have never led me to this completion. I would like to take this opportunity to express my thanks to all people who supported me.

First and foremost, I give sincerest thanks to my family who ever encouraged me from the beginning of the study. Without the support from them, I would never be in Delft experiencing a grateful moment and accomplish the Master's degree in TU Delft.

I express my gratitude to my daily supervisor Peter-Paul Harks. As a beginner in battery research I may have also asked many silly questions and his guidance has supported me so that I don't get lost during the thesis preparation. In daily experiments, he has helped me a lot from the basic knowledge of experiments, battery assembly to analysis. There were always good times and bad times in the experiments, when the results came wrong he encouraged me every time. I truly appreciate his supervision and patience. I attribute the level of my Master's thesis to his encouragements and attentions, I would have never completed my thesis without his help.

Furthermore, I would like to acknowledge my supervisor Prof. Dr. Ir. Fokko Mulder. I remember that his office was always busy, nevertheless he tried to find the time so that we could have a discussion. The knowledge he shared and suggestion helped me to widen my insight. I thank him for all the feedbacks I received for the thesis project.

In addition, I would like to extend my gratitude to Ir. Frans Ooms, Ing Michel Steenvoorden. I used many equipment for my thesis research, their kindness and help could accelerate my experiments. What's more, I would like to thank Thomas who helped and share his knowledge with me on Neutron Depth Profiling technique.

Finally, I give sincere thanks to my friends and colleagues. Especially, Bora, Jay, Xueyuan, Yifeng, Yuchen, Linmeng, Mengrou, Jiayao, Rendong, Pei, Valentina, Parth, Ivan, and Jing, thank you very much for making good memories in Delft and helping me a lot when I was in an extremely dark period. And thanks to my friends in China who were always accompanying with me through WeChat every day, keeping sharing funny things with me during the past three years. To my colleagues in RID, it was more fun and less lonely of having people in the office and lab. Not to mention, it was very nice to have talks about batteries during the coffee and cake time. :P

Thank you all and thank you for your interest in my Master's thesis!

Last but not least, Jing, we miss you. <3

Abstract

Due to the ascending of energy consumption and the development of renewable energy technologies, energy storage techniques has become a significant solution to match the increasing electricity generation. Among all the energy storage systems, the rechargeable battery is one of the most widely used technologies in industry and daily life.

Recently, rresearchers have been focusing on Li-S batteries for their high specific capacity (1675 mAh/g) and energy density (2600 Wh/kg). However, the polysulfides dissolution problem in the cell induces a fast capacity degradation issue which impedes Li-S battery to be brought into realistic commercial market.

In this thesis, attempts will be made to improve Li-S batteries by the incorporation of high specific surface area materials in the sulfur electrode to enhance adsorption of polysulfides as to prevent active material loss. Furthermore, the working principle of the lithium sulfur battery will be investigated through in-situ Neutron Depth Profiling.

Key words: Li-S battery, polysulfides adsorption, in-situ, NDP

Table of Contents

1

Introduction

1.1 Renewable Energy

Energy consumption has been an issue through the long history of civilization **[1]**. From the invention of steam engines to the emergence of automobiles, innovative technologies have increasingly demanded various source of energy to be transformed into socioeconomic benefits **[2, 3]**. Traditionally, fossil fuels have long been the main, if not sole, source of energy **[4]**. As technology advances and with the world population growing at a tremendous rate, fossil fuels may not sustain our needs for long. According to *International Energy Outlook 2016*, energy consumption has reached a record of 549 quadrillion Btu, while the fossil fuel reserves may only support us until 2112 **[5]**. In addition, global warming issues caused by greenhouse gases emitting are becoming increasingly server **[6]**. Therefore, renewable energy has become a trending solution to satisfy this impeding need for sustainable clean energy **[7]**.

The development of renewable energy is extraordinary **[8]**. REN21 reported that the power sector from renewable sources grew from 17% in 2004 to 23.7% in 2015, giving an annual capacity of 785 GW. Although the energy transition from fossil sources to renewable energy appears inspiring, renewable energy has its own hurdles to overcome. Solar and wind energy, being the two major renewable sources, face the challenges of unstable power generation **[9]**. The electricity generated by solar panels and aerogenerators fluctuates over time, which largely depends on the local weather, season, or day-night shift **[10, 11]**. Such fluctuation prevents the electricity to be fed into the power system directly, therefore storage methods are essential **[12]**. Electrical energy storage (EES) systems collect the electricity generated from renewable sources and combine into the power system at a consistent rate, which gives a variety of benefits from circumventing line or local faults to smoothing of loads and weather effects **[12]**. Depending on the materials and methods, the duration of storage ranges from few seconds to

several months, leading to a diversity of applications (**Table 1**) **[12]**. Nevertheless, the conflict between the increasing demand of electricity generation and its unmatched storage capacity largely resulted in the waste of surplus electricity production **[13]**. Therefore, technology advancement to revolutionarily enlarge the storage capacity is in urgent need.

Full Power Duration of Storage	Applications of Storage and Possible Replacement of Conventional Electricity System Controls.	Biomass.	Hydrogen. Electrolysis +Fuel Cell	Large Hydro	Compressed Air Energy Storage (CAES)	Heat Or Cold Store + Heat Pump.	Pumped Hydro	Redox Flow Cells.	New And Old Battery Technologies	Flywheel	Superconducting Magnetic Energy Storage (SMES)	Supercapacitor	Conventional Capacitor or Inductor
4 Months	Annual smoothing of loads, PV, wind and small hydro.	✓	✓	✓									
3 Weeks	Smoothing weather effects: load, PV, wind, small hydro.	✓	✓	✓									
3 Days	Weekly smoothing of loads and most weather variations.	✓	✓	✓	✓	✓	✓	✓					
8 Hours	Daily load cycle, PV, wind, Transmission line repair.	✓	✓	✓	✓	✓	✓	✓	✓				
2 Hours	Peak load lopping, standing reserve, wind power smoothing. Minimisation of NETA or similar trading penalties.	✓	✓	✓	✓	✓	✓	✓	✓				
20 Minutes	Spinning reserve, wind power smoothing, clouds on PV		✓	✓	✓	✓	✓	✓	✓	✓			
3 Minutes	Spinning reserve, wind power smoothing of gusts.		✓				✓	✓	✓	✓			
20 Seconds	Line or local faults. Voltage and frequency control. Governor controlled generation.							✓	✓	✓	✓	✓	✓

TABLE 1. Storage Technologies and Applications.

1.2 Energy storage

As an essential part of renewable electricity, the history of EES began in the early 20th century **[13]**. Beginning with lead-acid accumulator, EES has grown into a large family consisting of the pumped hydro system (PHS), battery energy storage (BES), compressed air energy storage (CAES), fuel cells (FCs), super-capacitors, flywheels, superconducting magnetic energy storage (SMES), and thermal energy storage devices (**Figure 1**) **[14]**. Depending on the EES technologies, each system possesses a unique profile of specific energy and specific power (**Figure 2**) **[14]**.

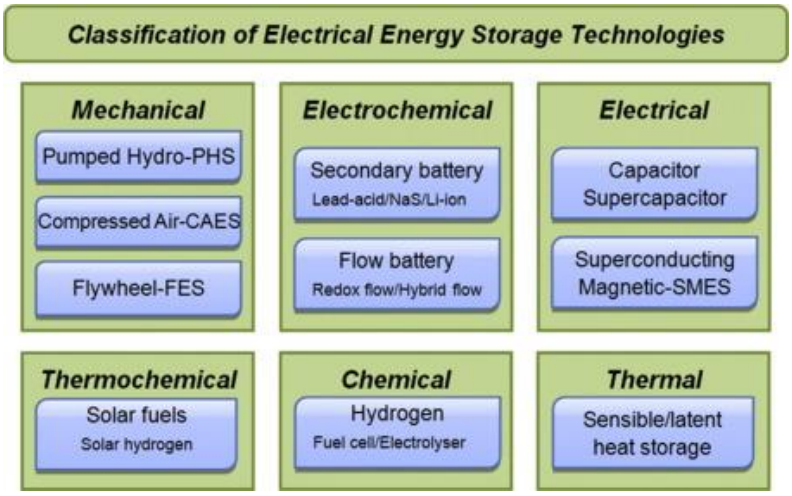

Figure 1. Classifications of EES technologies by the form of stored energy.

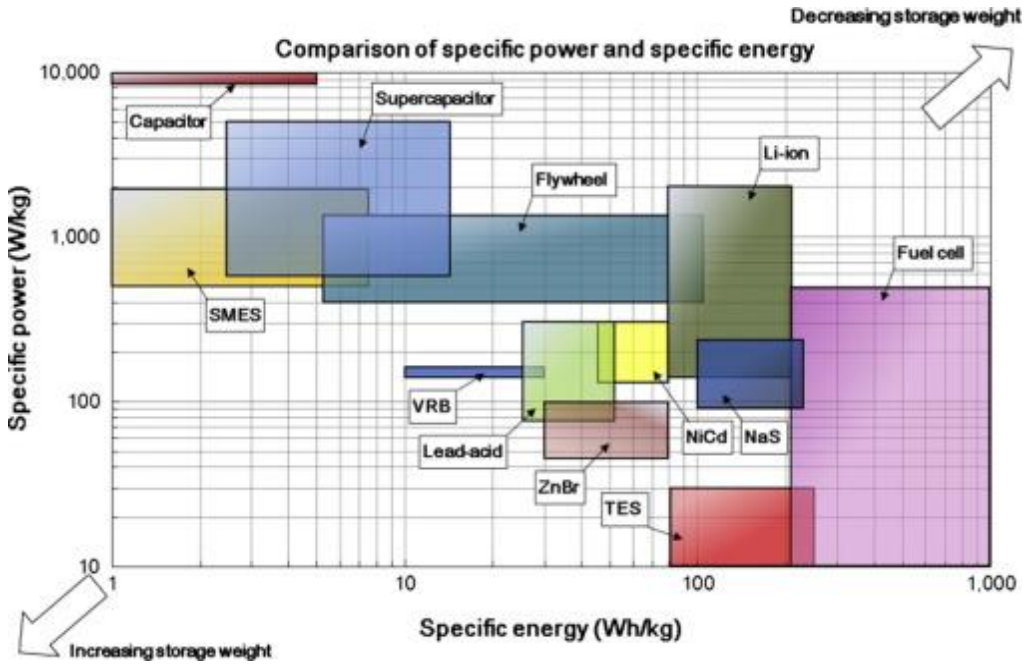

Figure 2. Comparison of specific energy and specific power.

Among all the EES, the rechargeable battery is one of the most widely used technologies in industry and daily life (**Figure 3**) **[14]**. Batteries are used in a large variety of applications with short construction time, ranging from power quality control to energy management **[14]**. Li-ion batteries are popular for their fast response time, small dimension, and high cycle efficiencies **[14]**. However, the theoretical intrinsic limit of energy density is limiting the future of Li-ion batteries. To compensate this significant drawback, researchers have

been focusing on Li-S batteries for their high specific capacity (1675 mAh/g) and energy density (2600 Wh/kg), which is 3-5 times higher than Li-ion batteries **[15]**.

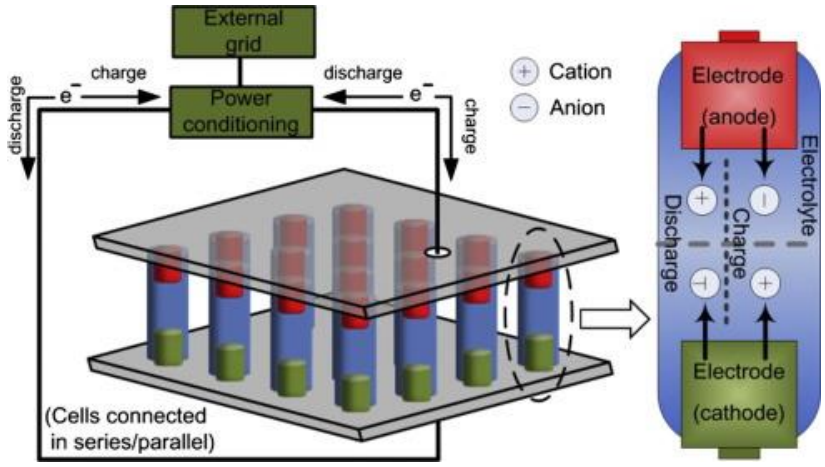

Figure 3. Schematic diagram of a battery energy storage system operation

Typically, Li-S cells consist of a sulfur/carbon composite cathode and a lithium metal anode with an organic lithium solution as electrolyte (**Figure 4**) **[15]**. Though promising, Li-S batteries face some unique challenges, from relatively minor ones such as the cathode volume change during operation, to major ones such as material depletion **[15]**. The polysulfide dissolution has been a main issue for the Li-S batteries, resulting to a rapid active material depletion which leads to a fast deterioration performance and poor cyclability. The problems and solutions will be explicitly elaborated in the next section.

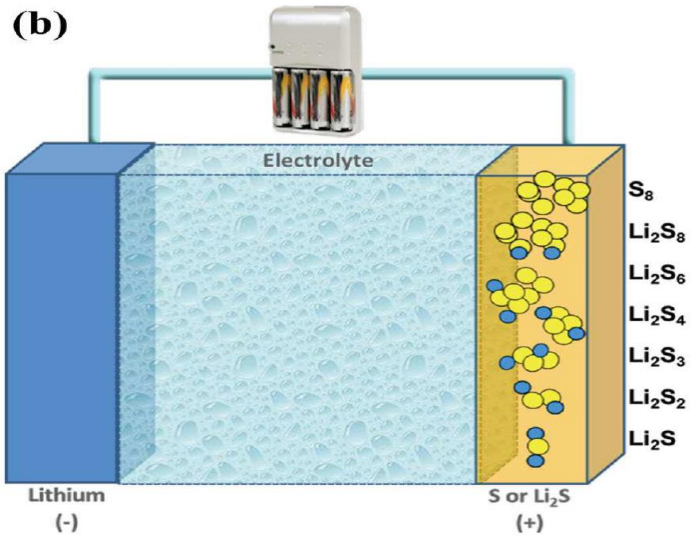

Figure 4. Schematic representation of a conversion reaction-based lithium sulfur battery.

1.3 Overview of the thesis

This thesis contains 6 chapters to tell the whole story of the project. The main purpose of this project is to improve the polysulfide adsorption by adapting different high specific surface area conductive material so as to prevent active material loss in the Li-S battery. In addition, an in-situ study of Neutron Depth Profiling will be investigated to visualize the lithium concentration variation in the sulfur cathode during discharge.

Chapter 1 introduces renewable energies and the significance of energy storage.

Chapter 2 explains the working principle, drawbacks and current solutions of Li-S battery.

Chapter 3 provides the preparation for the reference and comparison experiments.

Chapter 4 presents all experiments results and discussion related to battery performance.

Chapter 5 composes conclusions and recommendations for future research.

Chapter 6 focuses on the Neutron Depth Profiling measurements. Results, discussion and recommendations will also be addressed in this chapter.

The reference and Appendix present in the end.

2

Lithium Sulfur Batteries

In this chapter, the fundamental electrochemical reactions of Li-S batteries will be introduced; furthermore, the problems and current effective solutions will be elaborated on.

2.1 Basic Sulfur Chemistry

Being one of the richest elements in earth crust, sulfur (S) has increasingly attracted attention among EES researchers for its potential to be used as a novel cathode owing to its abundant, nontoxic and inexpensive merits **[16, 17]**. The most stable natural form of sulfur is cyclic α-octasulfur (α-S_8) which possess an orthorhombic structure **[16]**.

However, the poor electrochemical performances of sulfur impedes the direct utilization as a cathode material for Li-S batteries **[17]**. The primary problem lies in the poor conductivity of sulfur for both Li-ions and electrons. The electronic conductivity is about 5×10^{18} S cm^{-1}. Consequently, a reduced size sulfur structure combing an intimate contact with a porous conductive host is required for the purpose of improving the electronic and ionic conductivity of the electrode **[18]**.

The sulfur redox reactions are solution-based charge reactions that are largely affected by the dissolution of the sulfur species into the non-aqueous liquid electrolyte used in Li-S batteries **[15]**. Though sulfur has a low solubility in organic solvents, the dissolution rate of sulfur is high enough to ensure the electrochemical reactions in the battery **[18]**. Contrary to elemental sulfur, the reaction products are highly soluble in organic solvents. Therefore, both the solubility of sulfur in organic solvents and the properties of polysulfide anions should be taken

into consideration when designing a Li-S battery. In addition, different polysulfide anions co-exist as mixtures in a dynamic equilibrium, due to their similar Gibbs free energies **[15]**.

2.2 Electrochemistry reactions in Li-S batteries

Typically, Li-S cells consist of a sulfur cathode, a lithium metal anode and an organic lithium solution as electrolyte (**Figure 5**), though a few novel systems have adopted Li_2S as cathodes which are coupled with a lithium-free anode for safety concerns **[15]**.

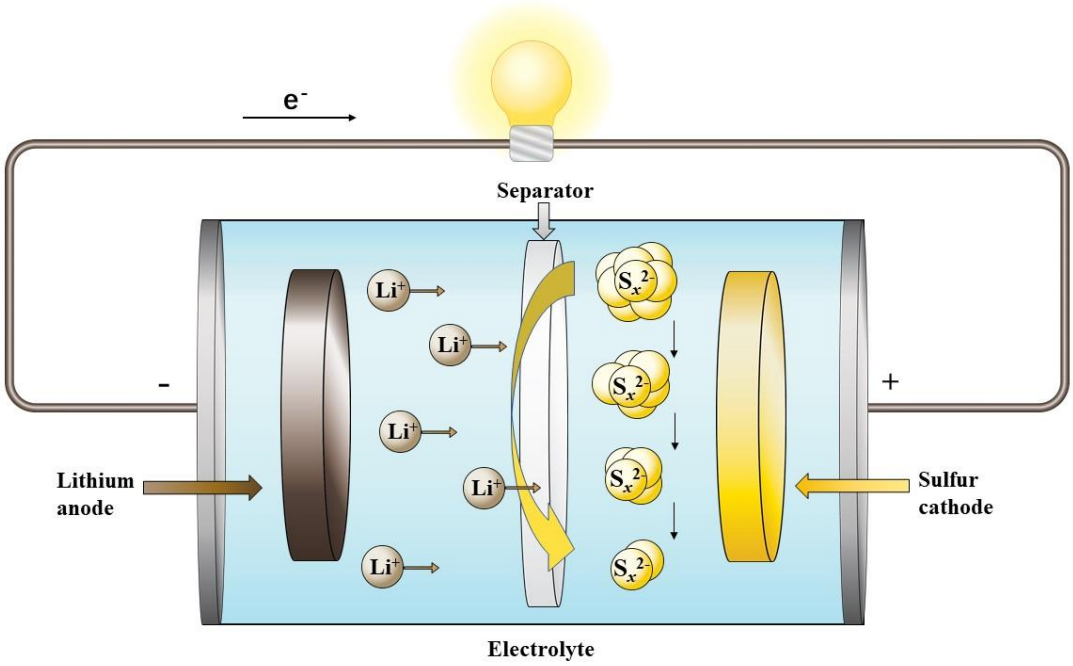

Figure 5. Illustration of the Li-S battery.

In both systems, discharging the cells reduces sulfur to Li_2S, while charging oxidizes it back to sulfur. The theoretical energy density with a potential of 2.15 V versus Li/Li^+ is determined by the overall reaction:

$$S_8 + 16Li \leftrightarrow 8Li_2S$$

The lower voltage compared to transition metaloxide-based intercalation reactions is compensated by the specific capacity of 1675 mAh/g, and therefore Li-S batteries have a much higher energy density than current Li-ion batteries **[15]**.

The Li-S electrochemistry is complex, involving multiple reaction steps. Depending on the electrolyte and reaction temperature, the (de)lithiation may consist of two or three stages (**Figure 6**) **[15]**. Reduction of elemental sulfur to higher-order polysulfides (Li_2S_x, $x \geq 4$) with a total discharge capacity of 419 mAh/g exhibits a plateau at 2.4 V, and the lithium polysulfide products can dissolve in a selection of electrolytes **[15]**:

$$S_8 + 2Li \leftrightarrow Li_2S_8 \qquad 2.39\ V\ vs.\ Li^0/Li^+$$

$$3Li_2S_8 + 2Li \leftrightarrow 4Li_2S_6 \qquad 2.37\ V\ vs.\ Li^0/Li^+$$

$$2Li_2S_6 + 2Li \leftrightarrow 3Li_2S_4 \qquad 2.24\ V\ vs.\ Li^0/Li^+$$

The high-order polysulfides are further reduced to low-order polysulfides (Li_2S_x, $1 < x < 4$) with a total discharge capacity of 1256 mAh/g, resulting in lower voltage (<2.1 V). Li_2S_2 and Li_2S are then precipitated on the cathode surface as an insulating layer **[15]**:

$$Li_2S_4 + 2Li \leftrightarrow 2Li_2S_2 \quad 2.2\ V$$

$$Li_2S_2 + 2Li \leftrightarrow 2Li_2S \quad 2.15\ V$$

Furthermore, Li_2S_x is unstable in organic electrolytes and may undergo disproportionation to form shorter Li_2S_y ($y < x$) **[15]**:

$$Li_2S_x \rightarrow Li_2S_y + (x\text{-}y)\ S$$

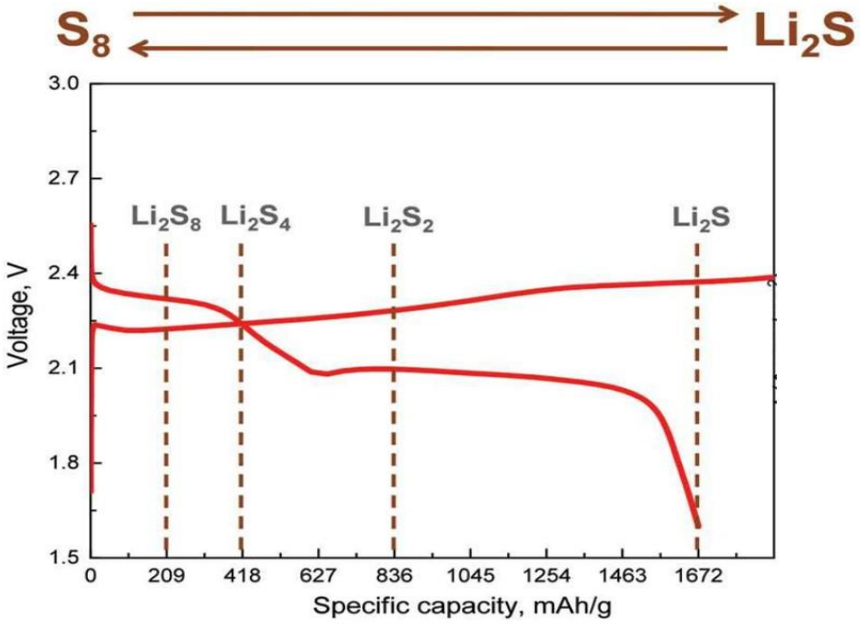

Figure 6. Illustration of the voltage profile and chemistry.

2.3 Problems of Li-S batteries

Although the Li-S system is a promising novel battery, it is still in technological infancy and many hurdles remain to overcome to achieve the level of performance for commercial application **[15]**.

2.3.1 Cathode Volume Change

The expansion of the active material volume upon cycling has been one of the key issues for Li-S batteries. The density discrepancy between sulfur (2.07 g/cm^3) and Li_2S (1.66g/cm^3) **[15]** leads to a volume change up to 80% when sulfur is fully converted **[15]**. Such a significant volume change may pulverize the active materials, resulting in rapid decay of capacity. Furthermore, commercial application demands high sulfur loading that cannot be achieved with such volume stretching. Studies have shown that large amount of conductive agent may function as a volume buffer when added in the electrodes to alleviate the deleterious effects caused by volume expansion/shrinkage **[15]**.

2.3.2 Sulfur Species Dissolution During Charge/Discharge

Another issue related to this battery is that polysulfide species dissolve in electrolytes at various stages, in addition to elemental sulfur which weakly dissolves in aprotic electrolytes. These dissolutions accelerate the sulfur reduction process, which is deleterious to battery life. Since the solubility of sulfur is higher than Li_2S in most organic solvents, the kinetics favors sulfur reduction over Li_2S oxidation despite the lower conductivity of sulfur. On one hand, excessive sulfur reduction directly leads to the loss of active material in the cathodes. On the other hand, dissolved polysulfides may precipitate back on the electrode surface to alter the morphology and accumulate internal strain of the cathodes in each cycle. Together, the effects sharply reduce the battery life cycle **[15]**.

2.3.3 Polysulfide Shuttle Reaction

The shuttle effect is also a major factor that affects battery performance. As dissolved polysulfide ions move from cathode to anode driven by the concentration gradient, long-chain polysulfides are reduced to short-chain polysulfides chemically at the surface of lithium anode:

$$(n\text{-}1)\ Li_2S_n + 2Li \rightarrow nLi_2S_{n\text{-}1} \quad \text{(chemical redox)}$$

The short-chain polysulfides then migrate back to cathode where they are oxidized to long-chain polysulfides again. This shuttling phenomenon occurs throughout the entire charging process and is affected by charge current and diffusivity. As a result, the battery shows high self-discharging and low coulombic efficiency, as the shuttling significantly prolongs the charging duration. Unfortunately, electrolytes with fast reaction kinetics frequently are good solvents for polysulfides which gives rise to severe shuttle problems, while Li^+ diffusion is generally poor for electrolytes with low solubility to polysulfides **[15]**.

2.3.4 Self-Discharge

The loss of the upper discharge plateau in the voltage profile of Li-S batteries indicates a rapid self-discharge, which is strongly undesirable for a practical EES. Due to the aforementioned polysulfide/sulfur dissolution and migrating issue that occurs even at the resting state, their reduction by lithium metal decreases the open-circuit voltage and the remaining discharge capacity **[15].**

2.3.5 Low conductivity of S and Li_2S

Elemental sulfur and stoichiometric Li_2S are intrinsically non-conducting, which requires a generous amount of conductive material to be added for their functionality as electrode. In addition, Li_2S_2/Li_2S precipitates on the sulfur surface during discharging, forming an insulating layer. Once the entire cathode is fully covered with the precipitation layer, cell voltage will decrease dramatically. Also, extra initiation energy is required when using Li_2S as the cathode material due to its low conductivity **[15]**.

2.3.6 Problems Associated with the Lithium Metal Anode

Lithium is generally extremely unstable in electrolytes as it reduces most electrolytes to form a solid-electrolyte interphase (SEI) layer continuously, which permanently decreases the capacity and anode efficiency. Lithium metal may also cause dendrite formation, which arguably may be suppressed with polysulfides and the application of $LiNO_3$ as an electrolyte additive. However, the reactions between lithium metal and dissolved polysulfide species creates additional problems, as they may corrode the anode, in addition passivate the anode due to the formation of the insoluble Li_2S and Li_2S_2. As a result, increased impedance and loss of active material will be induced **[15]**.

2.3.7 Electrolyte Depletion

Electrolyte depletion accounts for the majority reason for the low capacity and poor cycle life . Electrolytes may degrade due to attack of highly reactive polysulfide anions, or reactions between solvent molecules and polysulfides or lithium metal **[15]**.

2.4 Solutions to the Problems

As described above, the dominating problems in Li-S batteries are derived from the dissolution of polysulfide and consequent parasitic reactions. The redox shuttle which leads to a poor coulombic efficiency and undermines the morphology of lithium, only takes place during the charging process. While the parasitic reactions of the polysulfide, which have an impact on the capacity retention, self-discharge rate and safety problem, come along with the whole cycle

life of the battery **[19]**. It is because of the importance and inevitability of the polysulfide dissolution that researchers have spent effort on improving the chemical adsorption of polysulfide anions and on protecting the Li anode from reacting with soluble polysulfide **[19]**. Many techniques have been explored to fabricate the sulfur cathode with advantageous properties and structures to enhance the discharge capacity, cyclability and Coulombic efficiency **[20]**. For instance, high electronic conductivity materials (such as carbon) are combined with sulfur to enhance the electrical contact. Furthermore, elastic and porous substrates are applied to solve the volume variation problems of sulfur and to retain the polysulfide on the cathode **[17]**. Moreover, some other methods have been applied, such as novel cathode configurations with trapping interlayers, Li/dissolved polysulfide cells, and alternative electrolytes **[20-23]**.

The Sulfur-Carbon Composite Cathode

The fundamental drawback of Li-S battery derives from the extremely low electronic conductivity of sulfur impeding the cell to achieve its theoretical capacity, which can be solved by combing the carbonaceous material with sulfur. The main strategies have been pursued focusing on the improvement of carbon-based sulfur composites. Several beneficial requirements of the carbon matrix should be noted: (i) high electrical conductivity, (ii) electrochemical affinity to sulfur, (iii) high specific surface area or porous structure, (iv) liquid electrolyte accessibility to sulfur (v) strong framework to maintain the strain due to volume variation during the cycling process **[23]**.

Due to the structure diversity, the carbon materials can be categorized into several distinct groups, amorphous carbon (carbon black) **[24-26]**, macro-, meso-, micro-porous carbon **[27-31]**, carbon nanofibers **[32, 33]**, carbon nanotubes **[34-38]**, carbon spheres **[39, 40]**, and diverse types of graphite including expanded graphite **[41]**, graphene **[42-44]**, graphene oxide **[45]**, and reduced graphene oxide **[46]**.

Zhang et al. established a sulfur–carbon sphere composite cathode by thermal treatment of a mixture of sublimed sulfur and carbon spheres. The sulfur was highly dispersed inside the micropores of carbon spheres which had a large surface area and a narrow pore distribution. The sulfur-carbon sphere composite cathode with 42wt% sulfur presented an excellent high rate discharge capability and a large reversible capacity of 650 mAh/g after 500 cycles at

current density of 400 mAh/g, which was attributed to the strong adsorption of narrow micropores of carbon spheres **[40]**.

Schuster et al. synthesized a type of unique nanoscale spherical ordered mesoporous carbon (OMC) with highly bimodal porosities. The spherical OMC-sulfur composite cathode displayed a high initial discharge capacity of up to 1200 mAh/g at a current rate of 1C and good cyclability without compromising the rate capability **[47]**.

Jayaprakash et al. synthesized the hollow-structural carbon spheres which can constrain sulfur within the hollows like a "reservoir". Due to the electronically conductive feature of carbon, the electrochemical reactions between sulfur and lithium can be conducted inside the hollows. As a result, the composite electrode made of carbon spheres showed an excellent performance at both low and high current densities. The composites cathode with a sulfur content of 64.8% exhibited an initial specific capacity of 1071 mAh/g and maintained a capacity of 974 mAh/g at 0.5C after 100 cycles **[39]**.

Ji et al. prepared a graphene oxide-sulfur (GO-S) nanocomposite cathodes through a chemical reaction-deposition strategy. A thin sulfur layer was homogenously dispersed on the flake-like graphene oxide (GO) sheets and subsequently came along with a low-temperature thermal treatment process. The bulk sulfur coating on the surface of the GO layer melted and diffused into the pores of GO. The high surface area and strong adsorption properties enabled the polysulfide to be encapsulated into the cavities. Therefore, a high reversible capacity of 950-1400 mAh/g was demonstrated after more than 50 deep cycles at 0.1C (1C = 1675 mA g^{-1}) **[45]**.

Li et al. designed a carbon–sulfur nanocomposite coated with reduced graphene oxide (RGO). An ultrathin graphene nanosheet (TG) with large specific surface area, high pore volume, good conductivity, and broad pore distribution was utilized to synthesize a TG–sulfur (TG–S) stack-up nanocomposite. By combing the RGO coating layer, the RGO-TG-S nanocomposite can effectively entrap the polysulfides, rendering a reversible capacity of 667 mAh/g after 200 cycles at a current rate of 1.6 A g^{-1} (0.95 C) with a coulombic efficiency of 96% **[46]**.

Guo et al. synthesized the sulfur-impregnated disordered carbon nanotubes (SDCNTs) cathodes for the Li-S battery, which demonstrated a superior cyclability and Coulombic efficacy. Such achievement was attributed to the high temperature heat treatment of SDCNTs

in a vacuum environment, since the vaporized sulfur, S_6 or S_2 small molecules, can diffuse into the graphitized carbon layers and voids/defects in amorphous carbon where liquid electrolyte cannot penetrate easily which further alleviating the polysulfide dissolution **[35]**.

Ji et al. synthesized the porous carbon nanofiber-sulfur (CNF-S) composite electrodes by electrospinning, carbonization and solution-based chemical reaction-deposition method, which showed high reversible capacity, good discharge capacity retention and improved rate capability as cathodes in Li-S batteries. The high electrical conductivity and the extraordinary high surface area of the CNFs contribute to a good electrochemical performance. Sulfur can be dispersed homogeneously and immobilized into the porous structure. As a result, the polysulfide shuttle effect was ameliorated. The CNF-S composite cathode with a 42wt% S loading yielded an initial discharge capacity of 1400 mAh/g, 1100 mAh/g, 900 mAh/g at the current rate of 0.05 C, 0.1 C and 0.2 C, respectively. **[48]**.

Zheng et al. reported a hollow carbon nanofiber-encapsulated sulfur cathode which can effectively trap the polysulfides, consequently demonstrating a high specific capacity and extraordinary electrochemical performance. Anodic aluminum oxide (AAO) templates were utilized to fabricate the hollow carbon nanofiber arrays through a thermal polystyrene carbonization process. Sulfur was only coated onto the inner wall of carbon fibers with the help of AAO templates. In this way, polysulfides can be effectively confined into the hollow structures which eventually alleviates the dissolution problem and reduces the volume variation. In the meantime, the thin carbon wall allows rapid transport of lithium ions. The cathodes exhibited a good cyclability and reversibility, still presenting a specific capacity of 730 mAh/g after 150 cycles at the current rate of C/5 **[49]**.

Nevertheless, remarkable progress has been achieved with the help of these advanced carbon-sulfur composites cathodes, high active material loading (>70wt%), high specific capacity (>1200 mAh/g), and excellent cyclability (<10% capacity loss over 100 cycles) could not be acquired simultaneously among any abovementioned composite cathode **[23].**

Usually, a melt method or a solution method is used to prepare the sulfur-carbon composite electrodes. The melt method impregnates sulfur into the pores of carbon by thermal treatment

up to 160 ℃ when sulfur has the lowest viscosity **[28, 29]**. The solution method is based on dissolving solid sulfur into a solvent, for instance carbon disulfide carbon disulfide (CS_2), toluene, or dimethyl sulfoxide (DMSO), and then simply mixing carbon powders with the solution to absorb the dissolved sulfur **[25, 26]**. Various sulfur allotropes will be produced with different methods, while the performance of the composite cathodes will not be influenced since all allotropes will turn into α-sulfur at room temperature **[19]**.

3

Experiment Preparation

3.1 Purpose of the thesis

Based on some previous work, we can see researchers are mainly focusing on the improvement of utilization of carbon host. However, those approaches require complex processing techniques inducing high economical costs, which are not favorable for large-scale practical applications. This thesis has been focusing on trapping the dissolved polysulfide within cathode based on the physical adsorption and absorption, several porous conductive materials with various simple and low-cost mixing techniques have been applied to fabricate the sulfur-carbon composite cathode aiming for improving the Li-S batteries performance.

In this chapter, the general sulfur-carbon composite electrode preparation process will be introduced, and a Super-P carbon black based cathode was set as the reference electrode in this thesis. In total, eight sets of experiments have been conducted, which were carried out in a chronological order as follows:

1) Reference cathodes preparation

2) Comparison experiments:

   i) Porous carbon Tests

   ii) Carbon adsorption Test

   iii) No.25 carbon and Graphene as adsorber in cathode

   iv) Black phosphorus as adsorber in cathode

   v) Coin cells tests—reference, G15P15, No.1 and No.4 black phosphorus electrodes

   vi) Phosphorene as adsorber in cathode

3.2 Reference cathodes preparation

The reference composite electrode slurry was prepared by mixing 60wt% active material sulfur (300mg, >99.9%, Sigma-Aldrich,), 30wt% Super-P carbon black (150mg, Timcal) as a conducting agent, 10wt% Polyvinylidene fluoride (50mg, PVDF, Sigma Aldrich) as a binder in N-Methyl-2-pyrrolidinone (NMP, 99.5% anhydrous, Sigma Aldrich) as solvent. The mass of the solvent was 3-4 times of the total solid mass. The mixing process was divided into two steps. Firstly, 50mg binder and a certain amount of NMP (around 700mg-800mg) were mixed in a small glass vessel by magnet stirring for half hour till the binder completely dissolved. Then, 300mg sulfur, 150mg carbon and the remnant amount of solvent (around 800mg-1200mg) were added separately and were stirred for overnight until a homogenous slurry was obtained. The resulting slurry was casted onto a piece of aluminum foil by a doctor blade with a thickness of 200μm. The aluminum foil acts as a current collector. The casted foils were dried in the fume hood at room temperature for overnight and afterwards dried in the vacuum oven at 60℃ for two hours. Next, to improve the electronic contact between active material (sulfur), conductive agent (carbon) and current collector (aluminum foil) **[50]**, the foils were mechanically compacted quickly by a roller compressor under 1MPa and then cut into circular pieces by a 12.7mm diameter cutter. Furthermore, those circular pieces were dried in the vacuum oven for one hour and then on the heater inside the glovebox for overnight with the temperature of 55℃-60℃ to evaporate the NMP completely, and remove all residual water. The mass loading of the dry cathodes was about 1.5 mg/cm^2.

3.3 Assembly of batteries

The two-electrode lab cell was assembled in the argon filled glovebox with water and oxygen concentration under 1ppm (**Figure 7**). Lithium metal was used as the counter electrode and reference electrode. The separator was whatman glasfiber or microporous polypropylene (Celgard 3401). The liquid electrolyte was made of 1.0 M lithium bis(trifluoromethane) Sulfonimide (LiTFSI) in 1,2-Dimethoxyethane (DME) and 1,3-dioxolane (DOL) (DME: DOL=1:1 in volume), with 2 wt% $LiNO_3$ as additive.

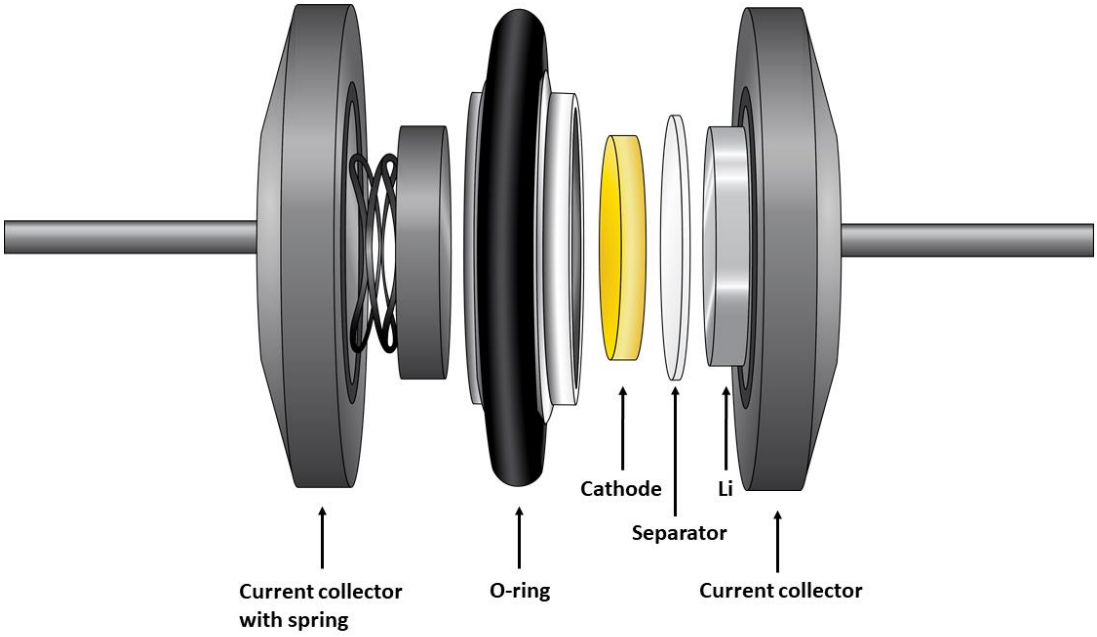

Figure 7. Illustration of an open lab cell with the components in place

3.4 Electrochemical measurement

The batteries after cell assembly were rested for two hours before the cycling test to wait for the open circuit potential to be stable. The charge/discharge cycling performance was studied on the Maccor 5300 battery test system software under a galvanostatic condition. The batteries were tested sequentially at C-rate of C/20 for 5 cycles, C/10 for 5 cycles, C/5 for 10 cycles, then back to C/20 for 180 cycles. The cut-off potential range was controlled between 1.8V and 2.6 V vs. Li^+/Li^0 at ambient temperature. The C-rate was calculated based on the theoretical capacity of sulfur and the amount of active material in each electrode (1C=1675 mA/g). The lithiation of sulfur is denoted as discharge and the delithiation process is defined as charge.

3.5 Comparsion experiments

3.5.1 Porous carbon tests

Five distinct types of experimental porous carbon were tested in this section, labelled as No.22, No.23, No.24 (graphene), No.25, No.26, which have high surface area compare to commercial Super-P carbon black. Some physical properties provided by the supplier (Cabot) are shown in **Table 2**. The slurries were prepared in the same composition and component proportions as

the reference slurry, except that Super-P carbon black was replaced by one of the experimental carbons. The mixing method, and subsequent coating, drying, pressing, cutting processes were the same as reference electrodes. The batteries were assembled in the same type of cells as the reference cells. The cycling procedure was the same as reference cells.

Carbon type	Particle size (nm)	Specific surface area (m^2/g)
Carbon black Super-P	15	150
EP10544-22	15	150
EP10544-23	17	200
EP10544-24 (graphene)	500-1000	700
EP10544-25	15	1500
EP10544-26	15	1400

TABLE 2. Physical properties of carbon particles. All the samples are from Cabot.

3.5.2 Carbon Adsorption Tests

For the carbon adsorption tests, to obtain a solution of 0.10 M Li_2S_6 in DME, proper amount of Li_2S (Sigma-Aldrich, 99%, anhydrous) and sulfur (Sigma-Aldrich, >99.9%), in a molar ratio of 1:5, were added to DME. For every carbon species from **Table 2**, 125mg of each powder was put in a vessel and dried in the vacuum oven for 24 hours. Afterwards, 3.0 mL of DME solution containing 0.10 M Li_2S_6 was added to each vessel, to measure the individual adsorption ability of the carbons towards the polysulfides. The mixtures were stored inside the argon filled glove box for 48 hours. The adsorption ability results were observed by eye based on the color change and the level of transparency of the samples.

3.5.3 No.25 carbon and Graphene as adsorber in cathode

Based on the adsorption tests, the No.25 carbon black and graphene showed a prominent adsorption ability. Thus, they were selected as carbon host additives, individually and mixed together with Super-P. The slurries were made of five components (Super-P carbon black, No.25 carbon black or graphene, sulfur, PVDF binder and NMP solvent). Four different composition proportions were tested, as shown in **Table 3**. The mixing method, and subsequent coating, drying, pressing, cutting processes were the same as reference electrodes. The batteries

were assembled in the same type of lab cells as the reference cells. The cycling procedure was the same as reference cells.

Battery	Super-P (wt%)	Carbon additives (wt%)	Sulfur (wt%)	Binder (wt%)
C25-5-P25	25%	5% No.25 carbon black	60%	10%
C25-15-P15	15%	15% No.25 carbon black	60%	10%
G5P25	25%	5% graphene	60%	10%
G15P15	15%	15% graphene	60%	10%

Table 3. Electrode compositions for Li-S batteries with carbon additives

3.5.4 Black phosphorus as adsorber in cathode

Properties of black phosphorus

Black phosphorus has been a promising negative material candidate for batteries owing to its high theoretical specific capacity (2596 mAh/g) property, which is about seven times larger than that of graphite. Besides, it also has a relatively good electric conductivity, exhibiting a mobility on the range of ~1000 $cm^2/V/s$ **[51]**. In addition, phosphorus presents a moderate chemical interaction with lithium polysulfides (Li_2S_x), which means the Li_2S_x can maintain intact and being trapped within phosphorus. Hence, the dissolution of Li_2S_x can be prevented in the electrolyte if phosphorus is applied in the Li-S batteries **[52]**. Therefore, we consider that by combing black phosphorus into reference cathode as an adsorber and conductive additive, the battery would present good conductivity, fast charge–discharge ability and stable cyclability.

Cathode preparation

Five various slurries were prepared by magnet stirring, with slightly different mixing steps to ensure black phosphorus was homogeneously dispersed in the slurries. The slurries were made of five components (Super-P carbon black, phosphorus, sulfur, PVDF binder and NMP solvent), in a same component proportion (58.5wt% sulfur, 30wt% Super-P carbon black, 1.5wt% black phosphorus, 10% binder). The mass of the solvent was 3-4 times of the total solid mass. These five slurries were labelled as from No.0 to No.4, the mixing techniques are as follows:

No.0 slurry: proper amount of binder was dissolved in certain amount of NMP solvent first. 30mg phosphorus was dispersed in 2ml NMP solvent then added into the prepared solution.

After magnet stirring for 30 minutes, sulfur and Super-P carbon black were added separately.

No.1 slurry: proper amount of reference slurry was prepared first. Then, 15mg phosphorus dispersed in 0.5ml NMP solvent was combined with the reference slurry and keep stirring for overnight.

No.2 slurry: proper amount of reference slurry was prepared first. Then, 15mg phosphorus dispersed in 2ml NMP solvent was combined with the reference slurry and keep stirring for overnight.

No.3 slurry: proper amount of binder was dissolved in certain amount of NMP solvent first. 15mg phosphorus was dispersed in 0.5ml NMP solvent then added into the prepared solution. After magnet stirring for 30 minutes, sulfur and Super-P carbon black were added separately.

No.4 slurry: proper amount of binder was dissolved in certain amount of NMP solvent first. 15mg phosphorus was dispersed in 2ml NMP solvent then added into the prepared solution. After magnet stirring for 30 minutes, sulfur and Super-P carbon black were added separately.

The subsequent coating, drying, pressing, cutting processes were the same as reference electrodes. The batteries were assembled in the same type of cells as the reference cells. The cycling procedure was the same as reference cells.

3.5.5 Coin cells—reference, G15P15, No.1 and No.4 black phosphorus electrodes.

Based on the results of previous batteries, the reference, G15P15, No.1 and No.4 phosphorus additive cathodes were selected to be assembled in CR2032-type coin cells. The cycling procedure was the same as reference cells.

3.5.6 Phosphorene as adsorber in cathode

Properties of phosphorene

Two-dimensional materials are considered as the most promising materials to replace traditional bulk materials, most recently, phosphorene has drawn great attention because of its superior physical properties and potential promising applications. Being similar to graphene, phosphorene is a one-layer or several-layer black phosphorus, can be produced from bulk black

phosphorus through various methods **[51]**. The Li_2S_x species adsorption and diffusion in a phosphorene monolayer was investigated by Zhao et al., showing that Li_2S_x species with long chains (Li_2S_8, Li_2S_6, Li_2S_4, and Li_2S_3) can be properly adsorbed on the phosphorene surface without altering the structures, preventing their dissolution into the electrolyte. Consequently, phosphorene is seen as a promising anchoring material for high-efficiency Li–S battery cathodes **[52]**. By adding phosphorene into the reference cathode as an adsorber, improved stability and cyclability are expected.

Cathode preparation

The slurry was made of five components (Super-P carbon black, phosphorene, sulfur, PVDF binder and NMP solvent), in a component proportion of 60 wt% sulfur, 28 wt% Super-P carbon black, 2 wt% phosphorene, 10% binder. The mass of the solvent was 3-4 times of the total solid mass. The slurries were coated onto aluminum foils by a doctor blade with a thickness of 100μm. The subsequent drying, pressing, cutting procedures were the same as reference electrodes. The batteries were assembled in CR2032-type coin cells. The cycling procedure was the same as reference cells.

4

Results and discussion

In this chapter, the results and discussion of reference and comparison experiments will be presented.

4.1 Reference cathode

Figure 8 shows the specific capacity as a function of cycle number for a typical Li-S cell, which will be taken as reference for the rest of the results shown in this chapter.

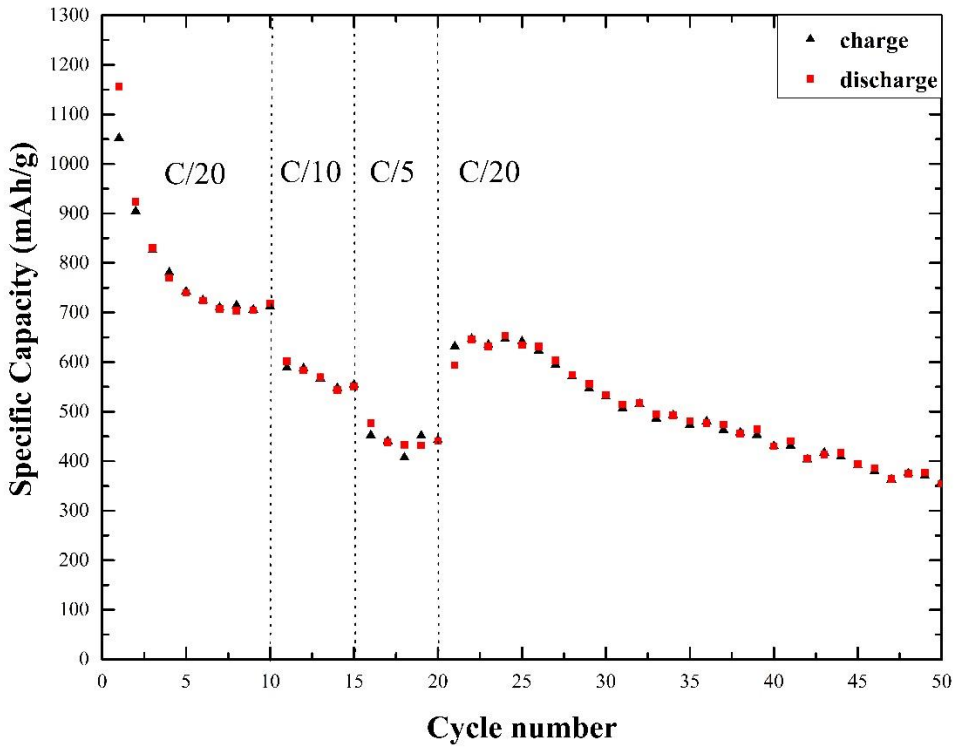

Figure 8. Reversible specific capacity *vs.* cycle number for reference cathode.

The initial reversible specific capacity was 1156mAh/g cycled with C/20, and after 10 cycles, the capacity steeply declines to 713 mAh/g. The reversible specific capacity stayed in the range of 500-600 mAh/g and 400-500mAh/g under the C-rate of C/10 and C/5 respectively, each for 5 cycles. When the C-rate turned back to C/20, the reversible specific capacity rose back to 654 mAh/g at the 24th cycle. But then a continuous and fast capacity decline showed up, indicating a rapid active material loss during the cycling process. After 50 cycles, the reversible specific capacity was 354 mAh/g, which was only 30% of the initial reversible specific capacity. The capacity loss per cycle was approximately 1.385%, which means the battery might be drained within 100 cycles. The capacity loss per cycle calculation was according to

$$\text{Capacity loss per cycle (\%)} = \frac{\frac{C_i - C_f}{C_i}}{\text{cycle number}} \times 100\%$$

It should be noticed that we have applied an easy and cheap method for the cathode fabrication, mainly focusing on the electrochemical performance in the Li-S batteries, with the intention of elucidating the mechanistic aspects (Chapter 6) and investigate the influence of different carbon additives on the performance. The simple mixing method might be one of the reasons for the rapid active material depletion in the cell. The sulfur particles in the cathode are quite large (>1 micron) applied without any sophisticated size-reduction technique. When the battery was in operation, large sulfur particles dissolved into the electrolyte, leaving relatively large voids in the cathode, resulting in a mechanically unstable structure of the cathode. No mechanism was in place to confine the polysulfides within the conductive materials, resulting in a fast active material loss during the cycling.

4.2 Comparison experiments

In this section, the results of the comparison experiments will be presented and analyzed in a chronological order.

4.2.1 Porous Carbon Tests

In this section, Super-P carbon black was replaced by various porous carbons in composite cathode. **Figure 9** shows the specific capacity as a function of cycle number for No.22, No.23,

N0,25, No.26 carbon black and graphene used as conductive material in Li-S battery.

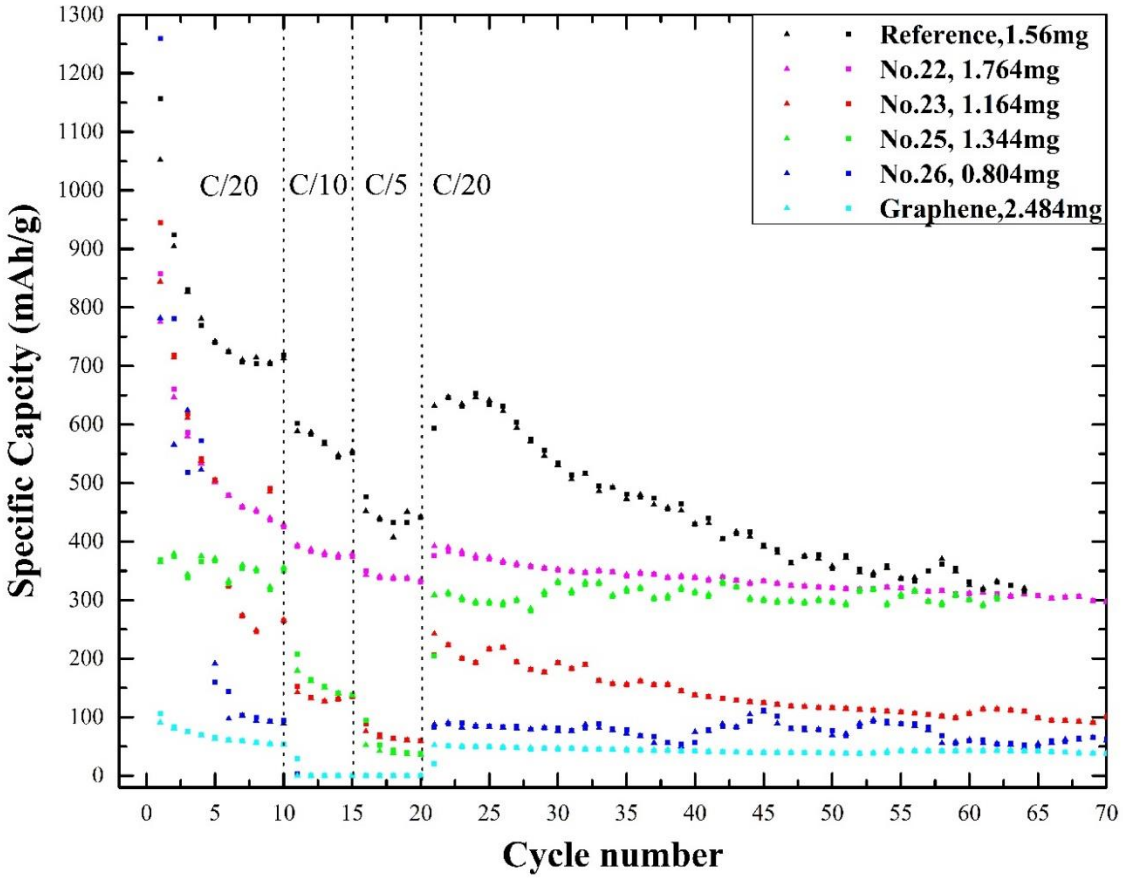

Figure 9. Reversible specific capacity *vs.* cycle number for various cathodes.

The initial reversible specific capacity cycled with a C-rate of C/20 is shown in **Table 4**.

Battery	No.22	No.23	No.25	No.26	graphene	reference
Initial specific capacity (mAh/g)	857	945	368	1258	105	1156

Table 4. Initial specific capacity comparison between various composite cathodes.

Compare to the reference cathode, only No.26 carbon black showed a relatively comparable initial specific capacity. However, the capacity dropped to 780 mAh/g in the second cycle, and then strikingly declined to 93 mAh/g in the 10^{th} cycle. While the reference cathode presented a specific capacity of 923 mAh/g in the second cycle, and still hold 718 mAh/g in the 10^{th} cycle.

Thus, the relatively comparable initial specific capacity of the No.26 carbon black was not representative for an improved battery performance result.

All the slurries were prepared in the same composition and component proportions as the reference slurry, except that Super-P carbon black was replaced by one of the experimental carbons. The mixing method, and subsequent coating, drying, pressing, cutting processes were the same as reference electrodes. However, the physical properties of the slurries were quite different from the reference slurry. The reference slurry had moderate liquidity and moderate viscosity, while the porous carbon slurries were too thin. Unlike the reference cathode, which was smooth and intact, the appearance of cathodes was coarse and fragile, some particles even detached from the cathodes. The inferior texture of the cathodes cannot provide a firm and steady circumstance for the electrochemical reactions. Therefore, it cannot be undoubtedly concluded that the low specific capacity and poor cyclability is an effect of the intrinsic properties of the experimental carbons.

Nevertheless, the cathodes with carbons showed a relatively stable capacity retention ability after 20 cycles. One speculation may explain this phenomenon, during the first 20 cycles, due to a loose structure of the cathode, mechanical cathode degradation was severe in the beginning, while after 20 cycles, the remnant carbons which stayed on the cathode firmly would provide a favorable frame to absorb the polysulfides. Hence, the cells degraded slowly from the 20^{th} cycle till 70^{th} cycle. Though exhibiting low specific capacity, the stable retention performance might indicate that the porous carbons have stronger polysulfides adsorption ability.

4.2.2 Carbon Adsorption Test

As can be learned from section 4.2.1, straightforward application of the experimental carbons is not a good approach to investigate their influence on the battery behavior. Therefore, a qualitative test was applied to determine the adsorption ability of polysulfides, to determine which carbons to zoom in on for further testing.

The carbon adsorption ability was deduced by the transparency degree of the polysulfide solution with various carbon species. Based on the assumption, the dissolved polysulfide can be absorbed by the carbon species within the porous structures, which means the initial turbid slurries would turn into relatively limpid after standing for a period. Thus, a lower turbidity indicates a stronger affinity of the carbon species towards the dissolved polysulfides. As shown in **Figure 10**, graphene solution presents the highest transparency, followed by No.25 and No.26 carbon black. Feasible carbon species were selected through this simply prescreening

for further electrochemical measurements. Therefore, graphene, No.25 and No.26 carbon black which exhibited highest adsorption ability were chosen for the next section.

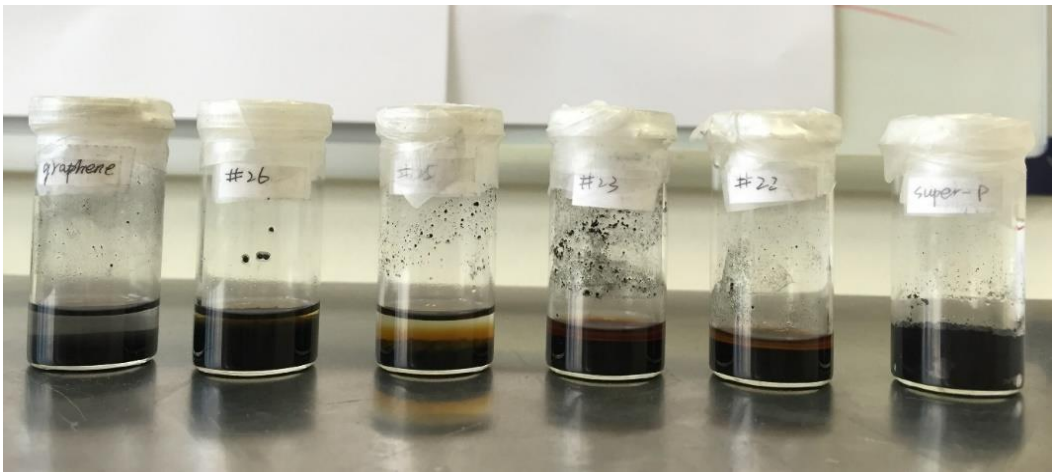

Figure 10. Results of carbon adsorption test. The carbon species are from **Table 2**.

4.2.3 No.25 carbon and Graphene as adsorber in cathode

Figure 11 shows the specific capacity as a function of cycle number for compsite cathodes with No.25 carbon black and graphene as adsorber.

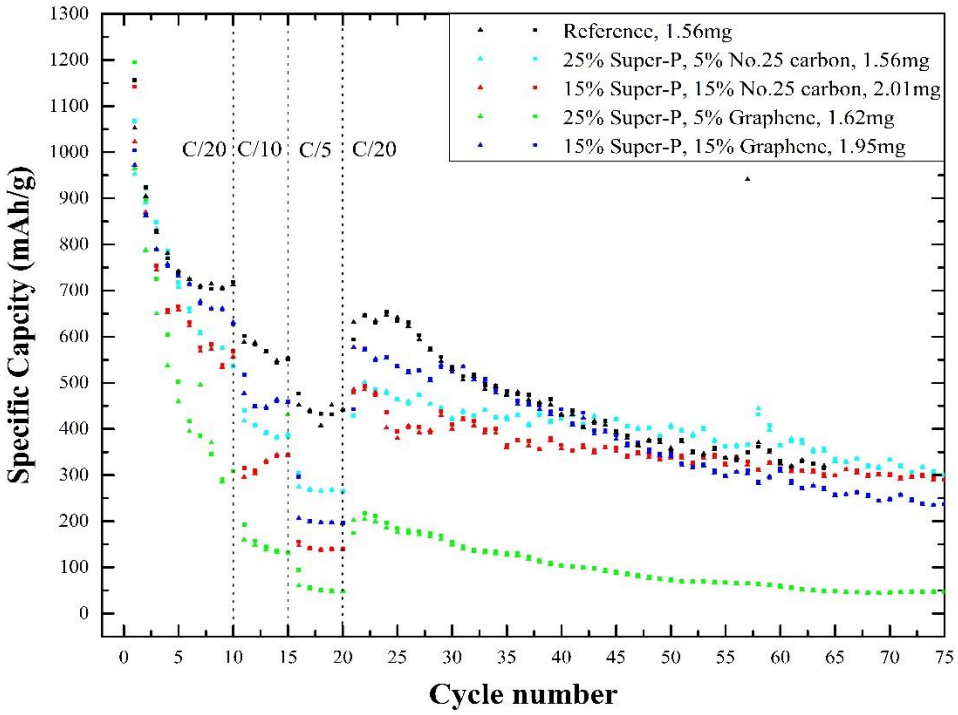

Figure 11. Reversible specific capacity *vs.* cycle number for various cathodes.

Based on the previous carbon adsorption tests, graphene and No.25 carbon black was selected to be added in the composite cathode as polysulfides adsorber, individually. Due to the inferior texture of the cathodes as discussed in section **4.2.1** when the porous carbons were applied as sole conductive material, the selected carbons were combined with Super-P carbon black to be the conductive host in the cathode.

The composite cathodes with porous carbon additives showed relatively comparable initial specific capacities, as shown in **Table 5**, which were much better than when the porous carbons were applied singly as conductive material is the section **4.2.1**. However, they all presented worse cycling performance compare to the reference cathode.

Battery	Super-P (wt%)	Carbon additives (wt%)	Sulfur (wt%)	Binder (wt%)	Initial specific capacity (mAh/g)
C25-5-P25	25%	5% No.25 carbon black	60%	10%	1067
C25-15-P15	15%	15% No.25 carbon black	60%	10%	1141
G5P25	25%	5% graphene	60%	10%	1194
G15P15	15%	15% graphene	60%	10%	1003
Reference	30%		60%	10%	1156

Table 5. Initial specific capacity of different composite cathodes cycling with C-rate of C/20.

For the batteries with No.25 carbon black as additive, in the first 10 cycles, they had similar degradation trend, when the C-rate was increased to C/10 and C/5, battery with 5% No.25 carbon as additive exhibited better rate capability compare to battery with 15% No.25 carbon as additive. When the C-rate came back to C/20, both presented slower specific capacity descending compared to the reference cathode. The former battery had a slightly better active material retention ability compared to the latter one, but the difference was not much. One reason that may explain this phenomenon, is that the weight of the former cathode was 1.56mg, while the latter one was 2.01mg. A lighter cathode indicated a thinner and more porous structure, thus a shorter travelling distance for the species was provided, and more active positions were present, resulting in better retainment of dissolved polysulfides. The conclusion can be drawn that the No.25 carbon additive does not make much contribution to the polysulfide adsorption in the composite cathode.

For the batteries with graphene as additive, the two cathodes had a distinct performance. For the battery with 5% graphene as additive, though the initial specific capacity was even higher than the reference cell, it dropped instantly and active material loss was severe. For the battery with 15% graphene as additive, it showed a similar cycling performance as the reference cell, and when the C-rate was changed to C/10 and C/5, the specific capacity dropped more compare to the reference cell did, indicating a slightly poorer rate capability. Though the weight of former cathode was lighter than the latter one, the performance was opposite, thus the previous reason was not applicable in this group. A speculation for the abnormal result was that the cathode appearance of with 5% graphene additive was coarse and lose, similar as the cathodes in section **4.2.1**, thus this battery had an inferior performance. In short, conclusion can be made that the graphene additive would not make much contribution for the improvement polysulfide adsorption in the composite cathode.

An interesting phenomenon was observed that, the more porous carbon additive added, the heavier the cathode was, which means the application of porous carbon would increase the density of the cathode, inducing less porous structures within the cathode. To maintain a firm structure, preferable porosity, and relative high energy density, further components composition of the slurry should be explored.

4.2.4 Black phosphorus as adsorber in cathode

Figure 12 shows the specific capacity as a function of cycle number for various composite cathodes with black phosphorus as adsorber being prepared in different methods.

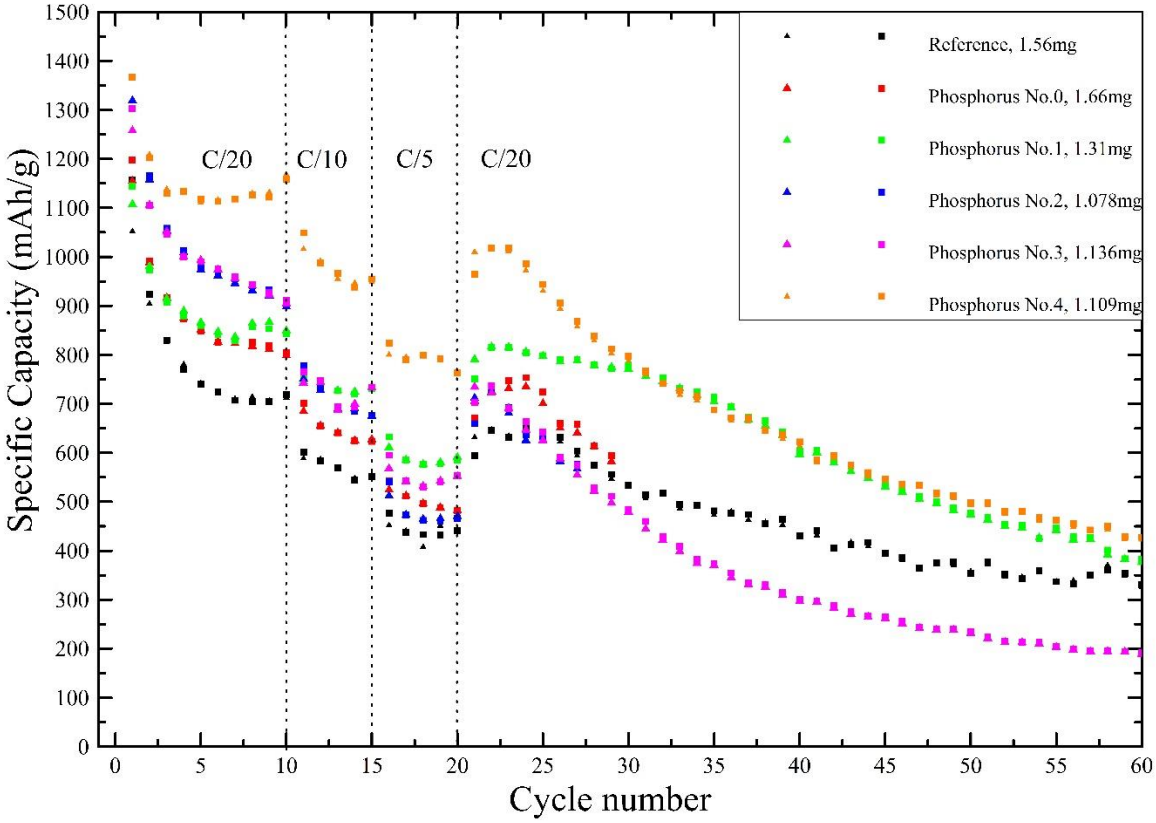

Figure 12. Reversible specific capacity *vs.* cycle number for various cathodes.

From No.0 to No.4 phosphorus additive cathodes, the initial specific capacity was 1197 mAh/g, 1144 mAh/g, 1367 mAh/g, 1302 mAh/g and 1366 mAh/g, respectively, which are equivalent or even superior compare to the reference cathode (1156mAh/g). It's obviously to see that in the first 20 cycles, all the phosphorus additive cathodes exhibited higher specific capacity and preferable rate capability than the reference cathode. The No.0 to No.3 phosphorus additive cathodes showed similar capacity decline trend. At the 10^{th} cycle, the specific capacity was 803 mAh/g, 842 mAh/g, 911 mAh/g, 911mAh/g, and 1158 mAh/g, from No.0 to No.3 cathode, respectively, which of the reference cathode was only 718 mAh/g. The capacity loss per cycle in the first 10 cycles for each type of cathode are shown in **Table 6**, apparently the reference cathode lost more active material during the first 10 cycles, while the phosphorus additive cathodes had better active material retention ability.

Battery	Reference	No.0	No.1	No.2	No.3	No.4
Specific capacity of 1st cycle (mAh/g)	1156	1197	1144	1367	1302	1366
Specific capacity of 10th cycle (mAh/g)	718	803	842	911	911	1158
Specific capacity loss per cycle in first 10 cycles (%)	3.78	3.29	2.64	3.33	3.01	1.52

Table 6. Specific capacity loss per cycle in first 10 cycles (%) comparison of reference and phosphorus additive cathodes.

For the No.4 phosphorus additive cathodes, the performance improvement was prominent. In the first 6 cycles, the specific capacity dropped to above 1100mAh/g, between 7th to 10th cycle, the specific capacity even rose back a little bit, and at the 10th cycle, the capacity still held 1158 mAh/g. After cycling under C/10 for 5 cycles and after cycling under C/5 for 5 cycles, the specific capacity was 954 mAh/g and 762 mAh/g, respectively, which were much higher than the performance of reference cathode. When the C-rate came back to C/20, the specific capacity reached back to 1018 mAh/g. Nevertheless, the following cycling performance still exhibited a rapid and steep decline.

As described in the experiment section, this cathode was prepared by uniformly dispersing black phosphorus into abundant NMP, then combing with binder dissolved NMP solvent. The solution would be used for subsequent slurry mixing with sulfur and carbon particles. Among all the phosphorus additive cathodes, though No.0-No.3 cathodes also showed improved electrochemical performance, No.4 cathode exhibited much superior capacity retention ability, thus the aforementioned slurry preparation method would be the optimal way to disperse black phosphorus homogenously into the normal composite cathode.

Based on the electrochemical performance analysis, it's reasonable to conclude that black phosphorus can be a promising adsorber material to enhance adsorption of polysulfides as to prevent active material loss in the Li-S battery.

4.2.5 Coin cells tests—reference, G15P15, No.1 and No.4 black phosphorus electrodes

Figure 13 shows the specific capacity as a function of cycle number for various cathodes tested in coin cells.

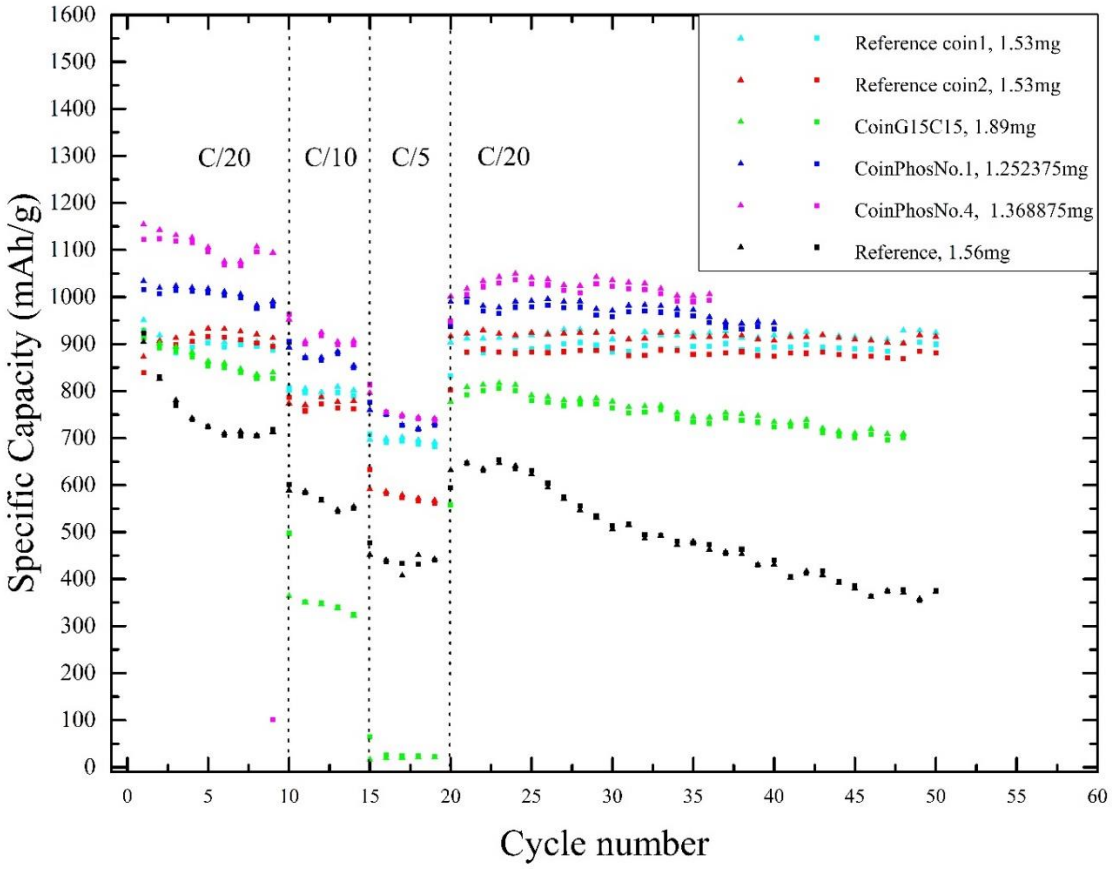

Figure 13. Reversible specific capacity *vs.* cycle number for various cathodes.

Although black phosphorus additive cathode displayed an enhanced performance, the poor cyclability was still a significant drawback in Li-S batteries. Assumptions were made by that the fast capacity descending was caused by two factors: firstly, the size of sulfur particles was too large which impeded the active material to be retained within the cathode; secondly, sulfur may react with the aluminum foil during the operation process which reduced the active material utilization. Therefore, several approaches including downsizing the sulfur particles and using carbon-coated aluminum foil as current collector were explored to solve the problem (see Appendix). However, the electrochemical performance still showed an inferior cyclability. Thus, CR2032-type coin cells were adopted instead of the lab-cells to cycle the Li-S batteries.

Based on previous results, several reference cathodes, a G15P15 cathode (15% graphene and 15% Super-P cathode as discussed in **4.2.3**) and No.1 and No.4 phosphorus additive cathodes were selected to be tested in coin cells.

As is shown in **Figure 13**, two reference coin cells presented relatively lower initial specific capacity, No.1 and No.4 phosphorus additive coin cells had equivalent initial specific capacity. Nevertheless, they all exhibited quite stable cyclability in the first 10 cycles. When the C-rate was raided to C/10 and C/5, the specific capacity still held more than 50% of the initial specific capacity, which was much higher compare to the reference cathode. When the C-rate back to C/20, the specific capacity of the aforementioned four cathodes all came back nearly equivalent to the initial specific capacity and can last for dozens of cycles, which means the active material loss was little. The above outcome indicated a remarkable cyclability and excellent rate capability.

For the G15P15 coin cell, though the initial specific capacity was relatively lower, but the active material retention ability was better than the reference lab cell, since after 10 cycles, the specific capacity of G15P15 coin cell was above 800 mAh/g, which of the reference lab cell as only around 700mAh/g. However, at a C-rate of C/10 and C/5, the specific capacity dropped suddenly to 350 mAh/g and 20 mAh/g respectively, indicating an inferior rate capability when the G15P15 cathode was applied in a coin cell. When the C-rate came back to C/20, the specific capacity rose back to 800 mAh/g and could still maintain more than 700 mAh/g after 45 cycles. This phenomenon demonstrated a superior cyclability but an inferior rate capability. An assumption was made to explain this poor rate capability, graphene may have a strong affinity regarding polysulfides, but the adsorption process is quite slow. Thus, this cell had dramatic difference of specific capacity under different C-rate.

An interesting observation was found that the coin cells had lower coulombic efficiency compare to the lab cell. The charging specific capacity was always slightly higher than the discharging specific capacity, which means the shuttle effect was happening during the charging process in the coin cells.

The superior cycling performance triggered us to investigate the reason why does the lab cell have a fast capacity degradation. Assumptions were made that there might be sealing or contact issue in the conventional lab cells. Extra experiments were conducted to explore the reasons (see Appendix), however no explanation could be found.

4.2.6 Phosphorene as adsorber in cathode

Figure 13 shows the specific capacity as a function of cycle number for cathode with phosphorene as adsorber tested in coin cells.

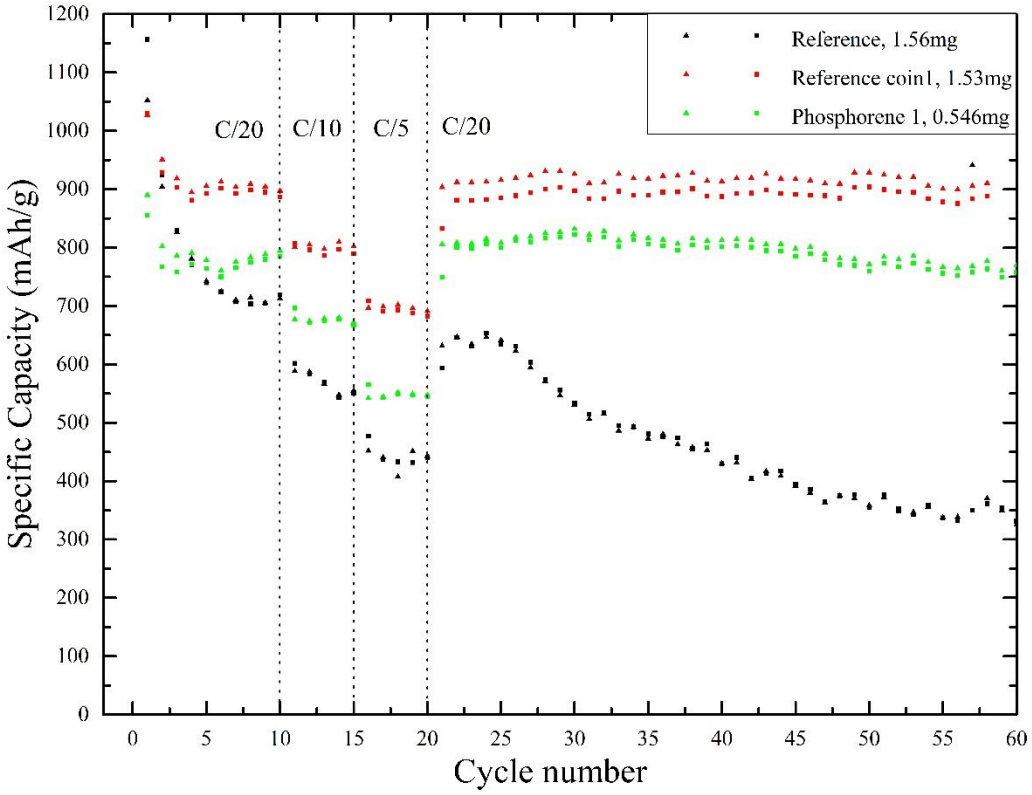

Figure 14. Reversible specific capacity *vs.* cycle number for various cathodes.

As is shown in **Figure 14**, the initial specific capacity of the phosphorene additive cathode was only 850 mAh/g, which was much lower than both the reference lab cell and the reference coin cell. Especially, in the first 3 cycles, the coulombic efficiency was quite lower indicating a severe shuttle effect, yet in the following 7 cycles, the specific capacity had a minor increase and the coulombic efficiency was also enhanced slightly. When the C-rate came to C/10 and C/5, the specific capacity was around 670 mAh/g and 550 mAh/g, respectively. When the C-rate sped down to C/20, the specific capacity came back to 800 mAh/g and after cycling for 60 cycles, the specific capacity still held about 750 mAh/g. The electrochemical performance showed a stable cyclability and favorable rate capability compare to the reference lab cell, but not as good as the reference coin cell. Overall, the improved cyclability and rate capability was primarily benefiting from the utilization of coin cell instead of the addition of phosphorene. The coulombic efficiency was improved compared to the reference coin cell, but not as good

as the reference lab cell. The severe shuttle effect accompanying the application of the coin cell got alleviated possibly due to the addition of phosphorene. The poor coulombic efficiency in the first 3 cycles may mainly because of the coin cell packaging, after 3 cycles, phosphorene was activated and its strong affinity towards polysulfides species could retain the active material within its structure and retard the highly order polysulfides migrating to the anode, thereby the shuttle effect got mitigated and consequently the coulombic efficiency was improved.

In addition, the mass active material of this cell was only 1/3 of the reference cells, that was because appearance of the cathode was thin and fragile. The specific capacity didn't get improved as the phosphorus additive cells did, which might because the inferior structure of the cathode instead of the intrinsic properties of phosphorene.

5

Conclusions and recommendations

5.1 Conclusions

According to the results from section **4.2.1**, the poor cycling performance mainly derived from the inferior texture of the cathodes. But a relatively stable retention ability presented from the 20th till 70th cycle indicate that the porous carbons might have stronger polysulfides adsorption ability.

Next, in the carbon affinity test, the transparency comparison results further confirmed that No.25 carbon black, No.26 carbon black and graphene certainly have high polysulfides adsorption ability.

However, the results from section **4.2.3** showed that the even combine with Super-P working together as conductive material and polysulfides adsorber in the sulfur cathode, the batteries still exhibited rapid capacity degradation, revealing that the spontaneously adsorption process was much slower compare to the cycling rate, thus no obvious improvement was seen in the battery.

From the results of section **4.2.4**, black phosphorus as adsorber in the cathode evidently improved the polysulfides adsorption within the cathode, though the batteries still presented a fast capacity fade after 25 cycles.

Remarkably, we found that coin cells presented much better active material retention performance compare to the lab cell, though the coulombic efficiency was relatively low indicating a severe shuttle effect in the coin cell.

In the end, phosphorene was combine with Super-P in the sulfur cathode tested in a coin cell. The specific capacity didn't get improved as the phosphorus additive cells did, which might because the inferior structure of the cathode instead of the intrinsic properties of phosphorene.

But an enhancement of coulombic efficiency was showed compare to the pure Super-P applied coin cell.

5.2 Recommendations

Based on the conclusions, some recommendations are addressed as follows:

Firstly, though Super-P carbon black didn't show an obvious polysulfides adsorption ability in the carbon affinity test, the reference cathode exhibited the best performance among most of the comparison experiment. More explorations can be conducted to find why Super-P has such an excellent performance compare to other high specific surface area carbons.

Secondly, though the electrochemical performance of porous carbons didn't show superior behavior than the reference cathode, strong adsorption ability indeed exhibited in the carbon affinity test, sophisticated techniques can be applied to insert sulfur into the porous carbons to further explore the merit of the advanced carbons.

Thirdly, though we've done several experiments to find the reasons why lab cell showed inferior cycling performance compare to coin cell, the rapid capacity degradation issue is still unsolved. More experiments should be carried out to solve the problem occurred in lab cell. If the reason is still unknown, suggestions would be made that choosing coin cell as priority.

6

Neutron Depth Profiling

6.1 Introduction of Neutron Depth Profiling

In situ, particularly in operando measurements, enable real-time monitoring of various chemical and physical processes, for instance, volume changes, phase transitions, side reactions, etc., while the battery is in operation without disassembling. Those phenomena can reflect the corresponding electrochemical reactions in the battery **[53]**.

In this section, an in-situ technique based on neutron depth profiling (NDP) was conducted to provide temporal and spatial measurement of Li within the Li-S battery and to visualize its transposition during the charging and discharging process. It is a nondestructive method for the real-time visualization and quantification of Li distribution. Here it is applied for the first time to explore Li-S batteries to shed light on the controversial electrochemical process during operation, which would provide valuable information to improve the development of Li-S batteries **[54]**.

The method works by bombarding a sample, such as a battery(electrode), with low-energy neutrons (~25 meV). The NDP technique is only sensitive to the ^{6}Li isotope. ^{6}Li, which has a natural abundance of approximately 7.5 at%, can absorb a neutron and subsequently emit an α-particle (^{4}He) and a triton (^{3}H), with defined energy, according to

$$^{6}\mathrm{Li} + n \rightarrow {}^{4}\mathrm{He}\ (2056.12\ \mathrm{keV}) + {}^{3}\mathrm{H}\ (2727.88\ \mathrm{keV})$$

By measuring the energy loss of the particles at the detector, the depth where the particles were formed can be deduced **[53, 55]**. The α-particles with 2+ charge can be utilized to acquire a high-resolution concentration profile of thin film batteries since they typically lose more energy when crossing the sample. On the other hand, triton particles can be used for measuring concentration profiles of thicker electrodes **[53]**.

The measurement should take place under a sub-ambient pressure to avoid energy loss owing to interaction with gaseous species on the way to the detector. Besides, no metallic casing is allowed and the thickness of the current collector should be as thin as possible since the produced α and triton particles can be intensively absorbed by metal **[53]**.

6.2 Experimental

Due to the requirements placed upon the battery, described in the previous section, a special cell needs to be configured to be able to conduct the experiments. The battery that was analyzed in this measurement contained a reference cathode mentioned earlier in this thesis. The reference slurry was coated on approximately 10.5 μm thick aluminum. After drying and pressing, the thickness of the cathode varied from 8to 20 μm. We took an average value of 14 μm for the quantification of the obtained data. A pouch cell with a circular window on cathode-side was assembled, consisting of a 14mm diameter lithium metal as the anode, a 4cm×4cm Celgard 3401 separator and the prepared cathode. In this way, the cathode current collector served as window for the NDP experiment. The separator was wetted with 0.5 mL electrolyte (The liquid electrolyte was made of 1.0 M lithium bis(trifluoromethane) Sulfonimide (LiTFSI) in 1,2-Dimethoxyethane (DME) and 1,3-dioxolane (DOL) (DME: DOL=1:1 in volume), with 2 wt% $LiNO_3$ as additive.).

The battery components were assembled under argon atmosphere (<0.1 ppm O_2/H_2O). The battery was rested for one hour before cycling so that the open circuit potential was stable. The electrochemical test was galvanostatically performed on the Maccor 4400 cycling system. Unlike the reference lab cell tested at ambient temperature and pressure, the pouch cell was operated under a vacuum condition with a pressure of 100 mbar. For the pouch cell, proper compression of the electrodes is more challenging than in rigid cells, and due to the sub-atmospheric pressure during the NDP experiments this potential problem is increased. The lack of compression on the battery-parts induces extra overpotentials compared to the reference cell. Thus, the cut-off potential range was set based on realistic overpotentials, and the battery voltage was no longer a reliable indicator of the state of charge. However, the battery was tested with constant currents for fixed periods of time, and therefore the amount of charge stored or drawn from the battery is known. The lithiation of sulfur is denoted as discharge and the delithiation process is defined as charge.

Neutron depth profiling was performed with one of the thermal neutron beam lines of the nuclear reactor of the Reactor Institute Delft. The NDP cell was positioned inside the vacuum chamber at an angle of 30° toward the incident neutron beam and parallel to the detector. The current collector of the cathode was facing to the neutron beam and the detector.

Because the stopping power of the current collector (10.5 μm Al foil) is too large for the α particles to leave the battery, hence, only the energy loss of the triton particles was measured with the charged particle Si detector. Next, the energy spectrum was collected by a multi-channel analyzer (MCA). A schematic representation of the in situ NDP measurement set-up is shown in **Figure 15**. The depth calibration, relating the measured ^{3}H energy to the Li-ion depth position, was computed by using a software named Stopping and Range of Ions in Matter (SRIM) **[55]**.

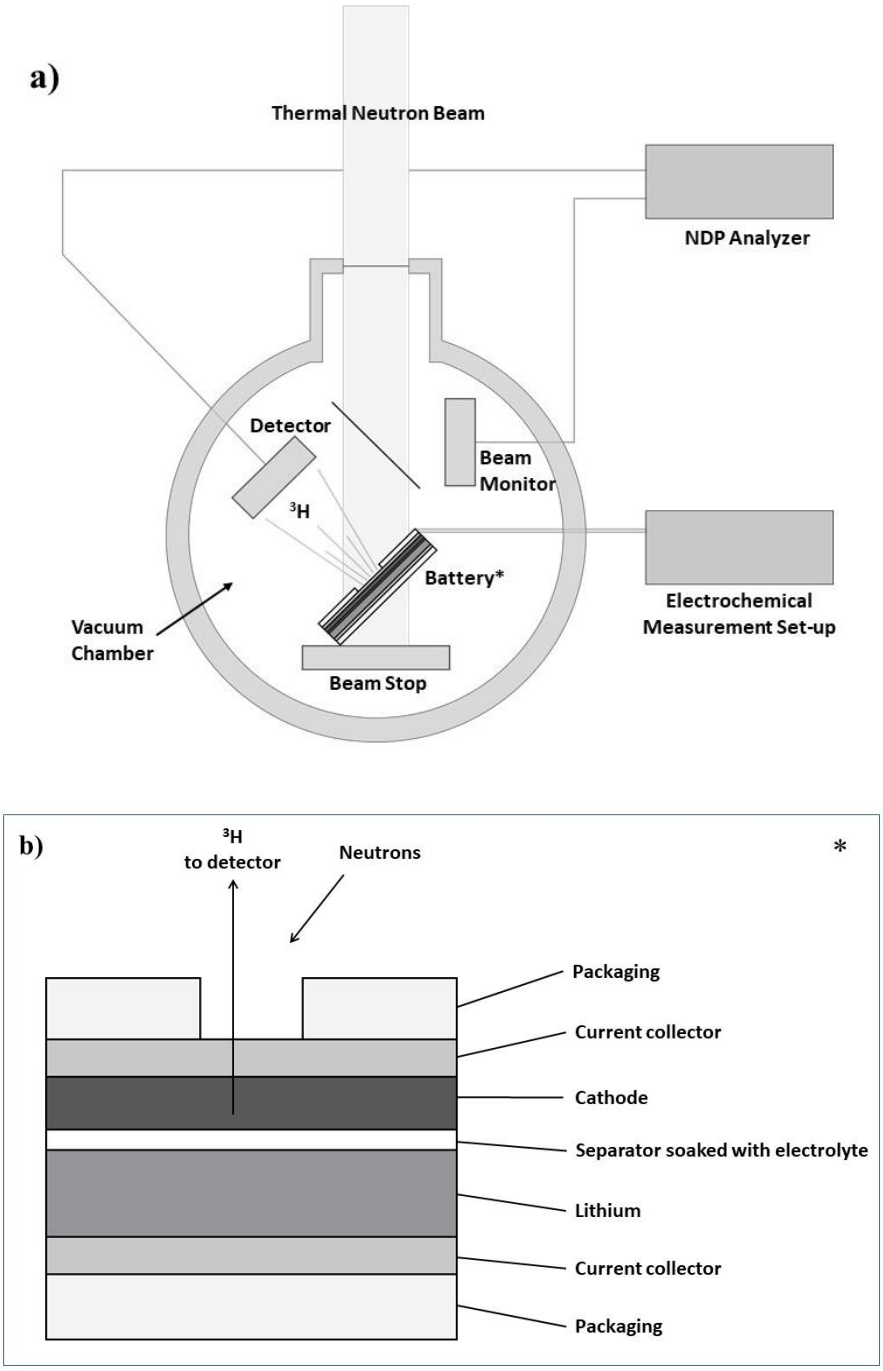

Figure 15. a) Schematic representation of the NDP set-up. b) The orientation of the battery inside the NDP measurement chamber.

6.3 Results and Discussion

Figure 16 shows a Depth-calibrated lithium intensity plot of the cathode and electrolyte. The depth profile is plotted so that zero depth correspond to the interface of the electrode and the current collector, and positive depth means inside the electrode or electrolyte.

The four different curves indicate four NDP measurements in a chronological order, starting from rest (pristine cell), followed by three periods of lithiation. The red curve denoted as D0 presented the Li-ion concentration during the rest time, no discharge happened, thus the corresponding intensity of D0, represents the Li^+ in the electrolyte. The flat plateau from cathode till electrolyte showed that the cathode was a porous structure, thus the electrolyte could penetrate the cathode and diffuse to everywhere.

The three upper level plateaus, denoted as D1, D2 and D3, presented three stepwise discharge processes, the increment of intensity indicated that during the discharge process, the Li-ion concentration was increasing. Due to kinetics reasons, a Li-ion concentration gradient was expected to be present in the cathode, however, these three plateaus were all relatively flat, indicating that the reaction was taking place in a catholyte environment, and the electrochemical reactions happened everywhere within the cathode.

It's worthy to notice that, the intensity level in the electrolyte side also increased along with the cathode side, which does not occur for conventional li-ion batteries. There, the Li concentration in the electrolyte remains equal to the start concentration as the same amount of Li-ions inserted into the electrolyte at the anode is taken up by the cathode. In the Li-S system, however, the partially lithiated active material can diffuse into the electrolyte, increasing the lithium concentration, which is indeed observed in our NDP measurement.

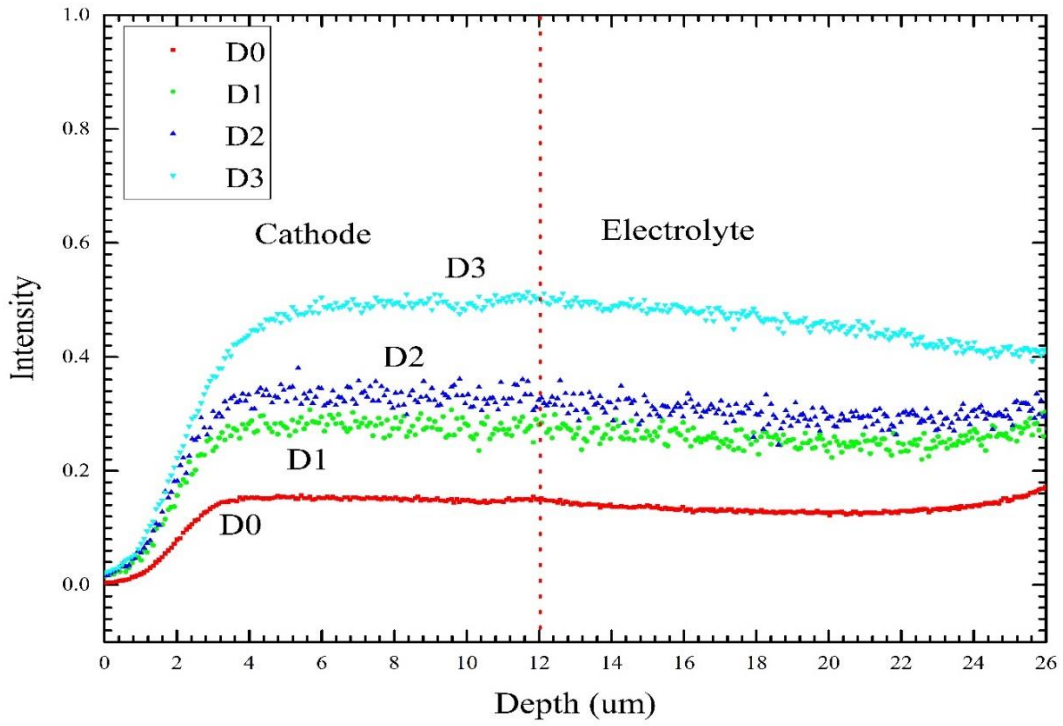

Figure 16. Depth-calibrated lithium intensity plot of the cathode and electrolyte

Figure 17 shows the specific capacity as a function of intensity measured from the detector. The intensity was associated with the Li ion concentration inside the cell. The specific capacity was derived from the electrochemical performance on Maccor 4400 cycling system. Four points shown in the figure, D0, D1, D2 and D3, indicate the four NDP measurements during rest and after three periods of discharge, respectively. Measurement D0 was conducted under rest conditions on the uncycled cell. Then the cell was cycling with a C-rate of C/20 for 2 hours. The specific capacity of D1 was around 170 mAh/g, leading to an intensity increase of 0.28 counts/sec. Next, the cell was continued cycling with a C-rate of C/20 for 1.25 hours, the specific capacity of D2 was 278 mAh/g and the corresponding Li-intensity rose to 0.33 counts/sec. Last, the cell was cycling with a C-rate of C/10 for 1 hours, the specific capacity of D3 was 421 mAh/g and the intensity rose to 0.49 counts/sec.

The red dot line through the four points, indicate that during the lithiation process, the specific capacity increases, the intensity will also ascend, in a linear fashion. Though the point of D2 is a bit off, overall, the intensity is linearly increasing along with the state of discharge.

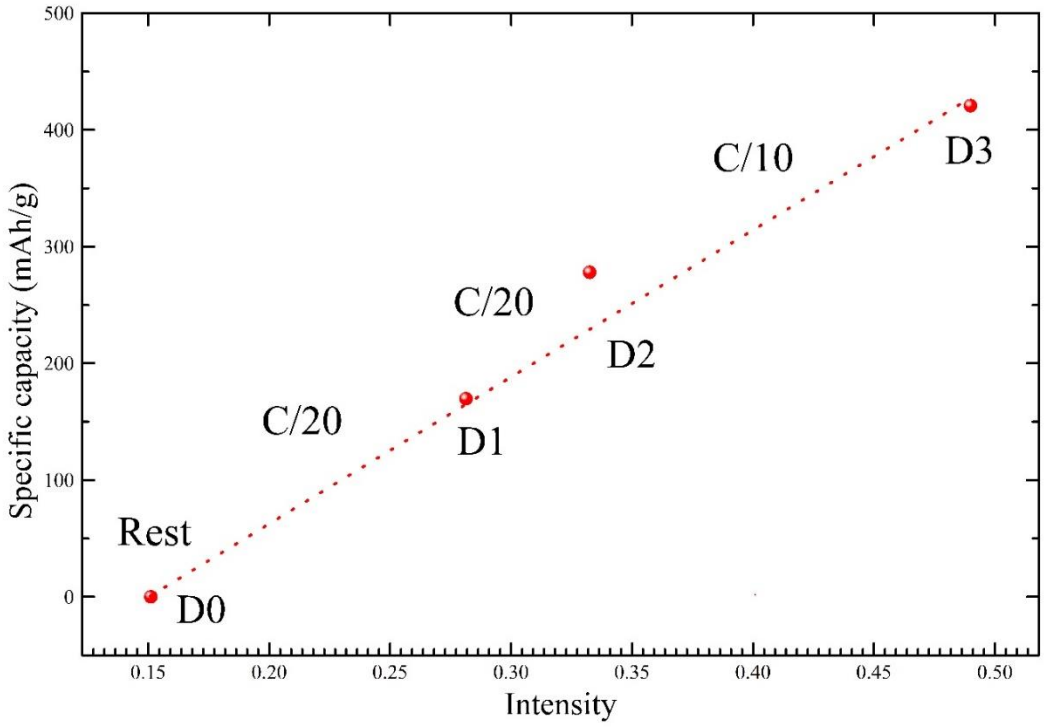

Figure 17. Li ion concentration variation during discharge

6.4 Conclusions and recommendations

In this section, the lithium increase in the sulfur cathode during discharging was visualized by adapting the in-situ study of Neutron Depth Profiling technique. The increasing intensity in the cathode during the discharge exhibited an accordance with the electrochemical process, and even the increase in lithium concentration in the electrolyte due to the emergence of polysulfides could be observed with this technique.

Due to a soft packaging texture of the pouch cell, the in-operando measurement it is currently challenging to connect the results to the electrochemical output of the battery. Further researches can focus on developing a both firm and adaptable cell to be applied in NDP measurements.

Appendix

1. Different approaches of making reference-slurry. (ball-milling, coating on carbon coated aluminum foil etc.)

The previous reference cathodes results showed a fast capacity decay, which might be influenced by two factors: Firstly, the sulfur particles were too large. During the cycling process, large particles dissolved into the electrolyte which inducing significant volume change and therefore resulting in a rapid decay of capacity. Secondly, the active material sulfur might react with the aluminum foil during the cycling process, thus reducing the practical active material utilization. To remedy the possible negative factors, several techniques were applied including downsizing the sulfur particles by balling-milling mixing method and preventing direct contact with aluminum by utilizing carbon-coated aluminum foil.

The slurries were coated onto aluminum foils by a doctor blade with a thickness of 200μm. The drying, pressing, cutting processes were the same as reference electrodes. The batteries were assembled in the same type of cells as the reference cells. The cycling procedure was the same as reference cells. The electrochemical performance is shown in **Figure 18**.

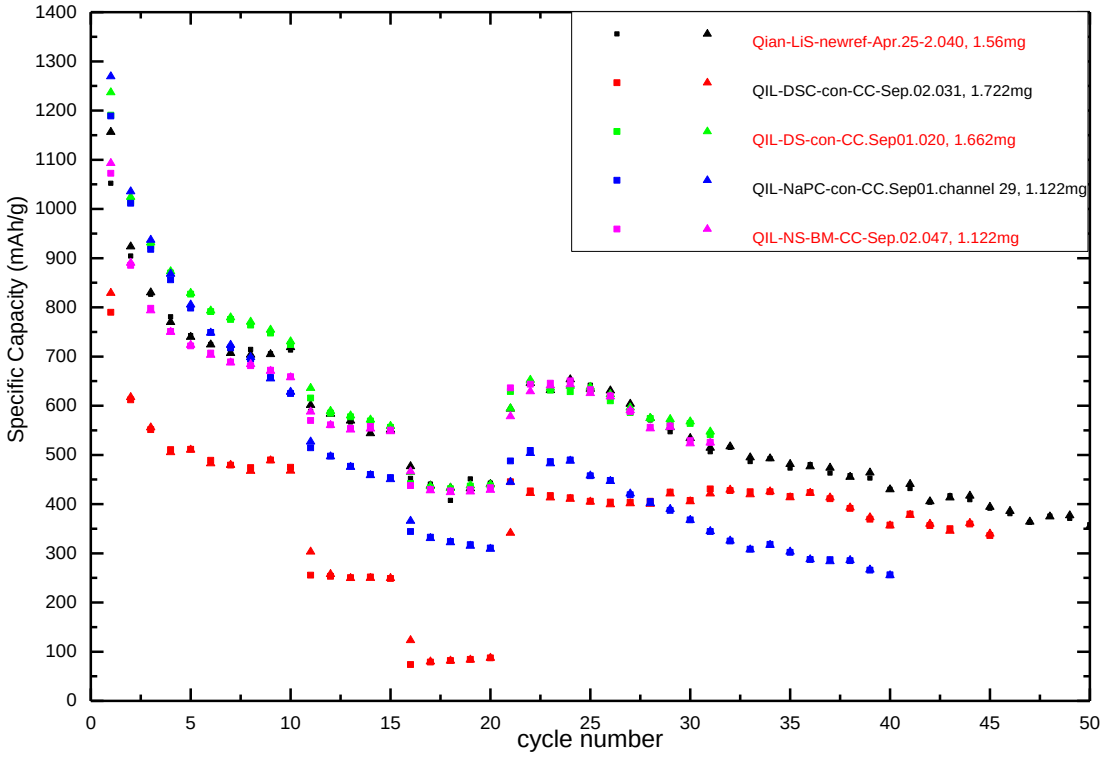

Figure 18. Reversible specific capacity *vs.* cycle number for various cathodes.

DSC-con-CC: Downsized (sulfur + Super-P) (ball-milling first), mixing in conventional way, coating on carbon coated Al foil

DS-con-CC: Downsized sulfur (ball-milling first) + Super-P, mixing in conventional way, coating on carbon coated Al foil

NaPC: Nano-sized phosphorus + Super-P + sulfur, mixing in conventional way, coating on carbon coated Al foil

NS-BM-CC: Normal sulfur + Super-P, ball-milling, coating on carbon coated Al foil

2. Sealing tests

From last section, all the coin cells showed better stability and cyclability compared to the previous corresponding cathodes tests in the lab cells. There might be sealing or contact issue in the conventional lab cells. To investigate the influence factors, two groups sealing tests were conducted based on the lab cell prototype, cycling in two different procedures separately. In the first group, a lab cell with a new O-ring covered with grease was applied to optimize the leakproofness was tested; besides, a lab cell with an extra layer of self-standing carbon membrane was inserted between the separator and the cathode was measured on the purpose of improving the polysulfide adsorption within the cathode. The cycling procedure was the same as the reference cathode. In the second group, a lab cell with 3 layers of lithium was tested to increase the internal pressure, a lab cell with extra smaller O-ring was operated to improve the airtightness. Besides, occasionally, some yellow residues can be seen deposited around the edge of lithium and separator when we open the tested lab cell, which means some polysulfides flowed away before participating the electrochemical reactions. This might be one of the reasons that the battery has a rapid degradation performance. Therefore, to solve this problem a lab cell with a lager lithium and larger Glasfiber separator was applied in the lab cell. In addition, a new reference cathode was conducted as benchmark. Batteries in this group were tested at the C-rate of C/5 for 200 cycles. The electrochemical performance is shown in **Figure 19**, **Figure 20.**

Reference cycling procedure

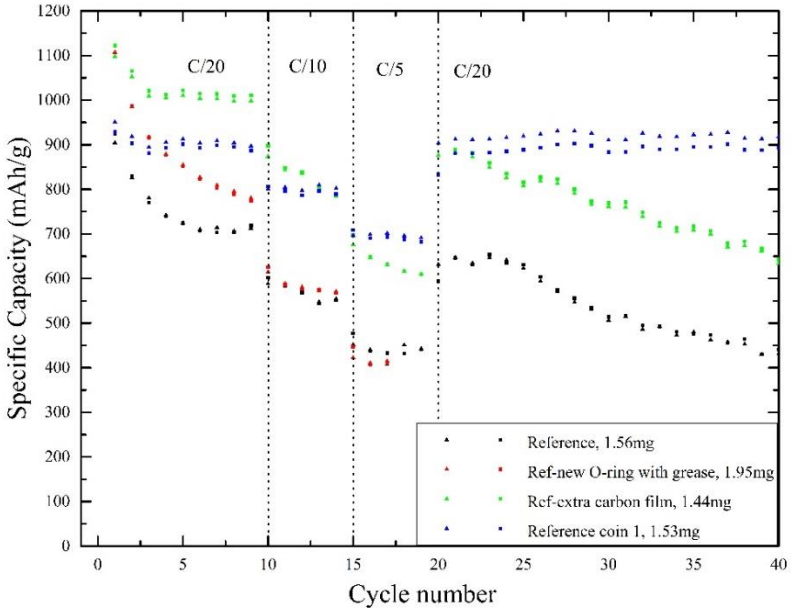

Figure 19. Reversible specific capacity *vs.* cycle number for various cathodes.

C/5 cycling procedure

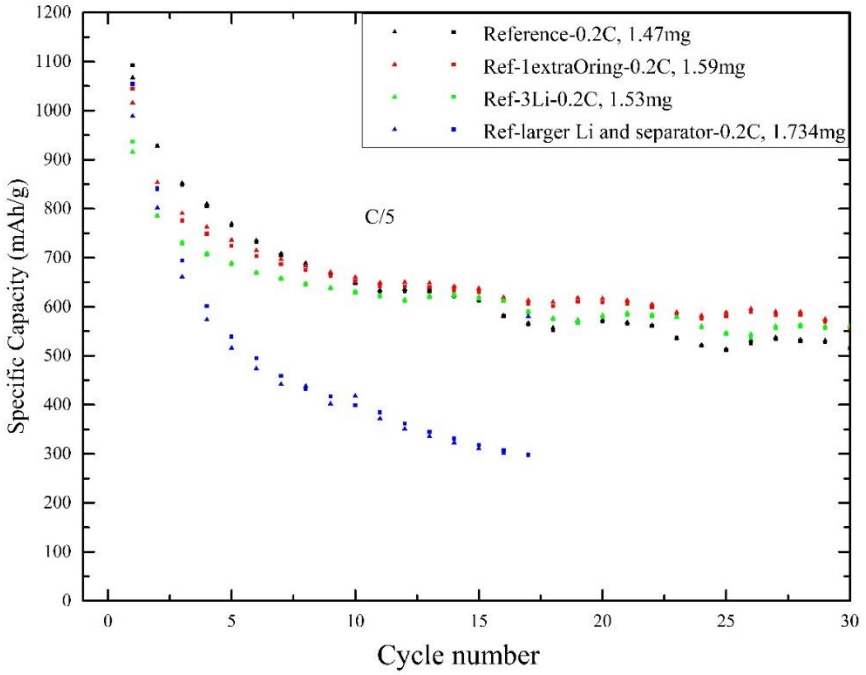

Figure 20. Reversible specific capacity *vs.* cycle number for various cathodes.

Reference

1. Smil, V., *Energy in world history*. 1994, United States: Westview Press, Boulder, CO (United States)].
2. von Tunzelmann, G.N., *Steam power and British industrialization to 1860*. 1978, Oxford: Clarendon Press.
3. Harvey, D.G. and W.R. Menchen, *Automobile: energy and the environment: a technology assessment of advanced automotive propulsion systems*. 1974, United States: Hittman Associates, Inc.,Columbia, MD.
4. Bartok, W. and A.F. Sarofim, *Fossil fuel combustion: A source book*. 1991, United States: John Wiley & Sons, New York, NY (United States).
5. Shafiee, S. and E. Topal, *When will fossil fuel reserves be diminished?* Energy Policy, 2009. **37**(1): p. 181-189.
6. Bauer, N., et al., *Global fossil energy markets and climate change mitigation - an analysis with REMIND.* Climatic Change, 2016. **136**(1).
7. Strantzali, E. and K. Aravossis, *Decision making in renewable energy investments: A review.* Renewable and Sustainable Energy Reviews, 2016. **55**: p. 885-898.
8. Sen, S. and S. Ganguly, *Opportunities, barriers and issues with renewable energy development – A discussion.* Renewable and Sustainable Energy Reviews, 2017. **69**: p. 1170-1181.
9. Jacobson, M.Z. and M.A. Delucchi, *Providing all global energy with wind, water, and solar power, Part I: Technologies, energy resources, quantities and areas of infrastructure, and materials.* Energy Policy, 2011. **39**(3): p. 1154-1169.
10. Cook, T.R., et al., *Solar Energy Supply and Storage for the Legacy and Nonlegacy Worlds.* Chemical Reviews, 2010. **110**(11).
11. Georgilakis, P.S., *Technical challenges associated with the integration of wind power into power systems.* Renewable and Sustainable Energy Reviews, 2008. **12**(3): p. 852-863.
12. Barton, J.P. and D.G. Infield, *Energy storage and its use with intermittent renewable energy.* IEEE Transactions on Energy Conversion, 2004. **19**(2): p. 441-448.
13. Yekini Suberu, M., M. Wazir Mustafa, and N. Bashir, *Energy storage systems for renewable energy power sector integration and mitigation of intermittency.* Renewable and Sustainable Energy Reviews, 2014. **35**: p. 499-514.
14. Luo, X., et al., *Overview of current development in electrical energy storage technologies and the application potential in power system operation.* Applied Energy, 2015. **137**: p. 511-536.
15. Xu, R., J. Lu, and K. Amine, *Progress in Mechanistic Understanding and Characterization Techniques of Li-S Batteries.* Advanced Energy Materials, 2015. **5**(16).
16. Meyer, *Elemental sulfur.* Chemical Reviews, 1976. **76**(3): p. 367-388.
17. Yin, Y.X., et al., *Lithium-sulfur batteries: electrochemistry, materials, and prospects.* Angewandte Chemie (International ed. in English), 2013. **52**(50): p. 13186-200.
18. Harks, P.P., et al., *The Significance of Elemental Sulfur Dissolution in Liquid Electrolyte Lithium Sulfur Batteries.* ADVANCED ENERGY MATERIALS, 2017. **7**(3): p. n-a-n-a.

19. Zhang, S.S., *Liquid electrolyte lithium/sulfur battery: Fundamental chemistry, problems, and solutions.* Journal of Power Sources, 2013. **231**: p. 153-162.
20. Su, Y.S. and A. Manthiram, *A new approach to improve cycle performance of rechargeable lithium-sulfur batteries by inserting a free-standing MWCNT interlayer.* Chemical communications (Cambridge, England), 2012. **48**(70): p. 8817-9.
21. Hassoun, J. and B. Scrosati, *Moving to a Solid-State Configuration: A Valid Approach to Making Lithium-Sulfur Batteries Viable for Practical Applications.* Advanced Materials, 2010. **22**(45): p. 5198-5201.
22. Zhang, S.S. and J.A. Read, *A new direction for the performance improvement of rechargeable lithium/sulfur batteries.* Journal of Power Sources, 2012. **200**: p. 77-82.
23. Manthiram, A., Y. Fu, and Y.S. Su, *Challenges and prospects of lithium-sulfur batteries.* Accounts of chemical research, 2013. **46**(5): p. 1125-34.
24. Zhang, B., et al., *Preparation and electrochemical properties of sulfur-acetylene black composites as cathode materials.* Electrochimica Acta, 2009. **54**(14): p. 3708-3713.
25. Li, K., et al., *Enhance electrochemical performance of lithium sulfur battery through a solution-based processing technique.* Journal of Power Sources, 2012. **202**: p. 389-393.
26. Liu, Y., H. Zhan, and Y. Zhou, *Investigation of S/C composite synthesized by solvent exchange method.* Electrochimica Acta, 2012. **70**: p. 241-247.
27. Chen, S.-R., et al., *Ordered mesoporous carbon/sulfur nanocomposite of high performances as cathode for lithium-sulfur battery.* Electrochimica Acta, 2011. **56**(26): p. 9549-9555.
28. Ji, X., K.T. Lee, and L.F. Nazar, *A highly ordered nanostructured carbon-sulphur cathode for lithium-sulphur batteries.* Nature materials, 2009. **8**(6): p. 500-6.
29. Lai, C., et al., *Synthesis and electrochemical performance of sulfur/highly porous carbon composites.* Journal of Physical Chemistry C, 2009. **113**(11): p. 4712-4716.
30. Li, X., et al., *Optimization of mesoporous carbon structures for lithium-sulfur battery applications.* Journal of Materials Chemistry, 2011. **21**(41): p. 16603-16610.
31. Liang, X., et al., *Highly dispersed sulfur in ordered mesoporous carbon sphere as a composite cathode for rechargeable polymer Li/S battery.* Journal of Power Sources, 2011. **196**(7): p. 3655-3658.
32. Choi, Y.-J., et al., *Improvement of cycle property of sulfur electrode for lithium/sulfur battery.* Journal of Alloys and Compounds, 2008. **449**(1): p. 313-316.
33. Rao, M., X. Song, and E.J. Cairns, *Nano-carbon/sulfur composite cathode materials with carbon nanofiber as electrical conductor for advanced secondary lithium/sulfur cells.* Journal of Power Sources, 2012. **205**: p. 474-478.
34. Ahn, W., et al., *Synthesis and electrochemical properties of a sulfur-multi walled carbon nanotubes composite as a cathode material for lithium sulfur batteries.* Journal of Power Sources, 2012. **202**: p. 394-399.
35. Guo, J., Y. Xu, and C. Wang, *Sulfur-impregnated disordered carbon nanotubes cathode for lithium-sulfur batteries.* Nano letters, 2011. **11**(10): p. 4288-94.
36. Jia, L., et al., *Polysulfides Capture-Copper Additive for Long Cycle Life Lithium Sulfur Batteries.* ACS applied materials & interfaces, 2016. **8**(44): p. 30248-30255.

37. Wu, F., et al., *Improvement of the electrochemical properties of sulfur cathode materials with multiwalled carbon nanotubes.* Carbon, 2011. **49**(5): p. 1806.
38. Zheng, W., et al., *Novel nanosized adsorbing sulfur composite cathode materials for the advanced secondary lithium batteries.* Electrochimica Acta, 2006. **51**(7): p. 1330-1335.
39. Jayaprakash, N., et al., *Porous Hollow Carbon@Sulfur Composites for High-Power Lithium-Sulfur Batteries.* Angewandte Chemie International Edition, 2011. **50**(26): p. 5904-5908.
40. Zhang, B., et al., *Enhancement of long stability of sulfur cathode by encapsulating sulfur into micropores of carbon spheres.* Energy & Environmental Science, 2010. **3**(10): p. 1531-1537.
41. Li, S., et al., *Layer Structured Sulfur/Expanded Graphite Composite as Cathode for Lithium Battery.* Electrochemical and Solid-State Letters, 2011. **14**(7): p. A105.
42. Wang, H., et al., *Graphene-wrapped sulfur particles as a rechargeable lithium-sulfur battery cathode material with high capacity and cycling stability.* Nano letters, 2011. **11**(7): p. 2644-7.
43. Park, M.-S., et al., *One-step synthesis of a sulfur-impregnated graphene cathode for lithium–sulfur batteries.* Physical Chemistry Chemical Physics, 2012. **14**(19): p. 6796.
44. Cao, Y., et al., *Sandwich-type functionalized graphene sheet-sulfur nanocomposite for rechargeable lithium batteries.* Physical chemistry chemical physics : PCCP, 2011. **13**(17): p. 7660-5.
45. Ji, L., et al., *Graphene oxide as a sulfur immobilizer in high performance lithium/sulfur cells.* Journal of the American Chemical Society, 2011. **133**(46): p. 18522-5.
46. Li, N., et al., *High-rate lithium-sulfur batteries promoted by reduced graphene oxide coating.* Chemical communications (Cambridge, England), 2012. **48**(34): p. 4106-8.
47. Schuster, J.r., et al., *Spherical Ordered Mesoporous Carbon Nanoparticles with High Porosity for Lithium-Sulfur Batteries.* Angewandte Chemie International Edition, 2012. **51**(15): p. 3591-3595.
48. Ji, L., et al., *Porous carbon nanofiber-sulfur composite electrodes for lithium/sulfur cells.* Energy & Environmental Science, 2011. **4**(12): p. 5053-5059.
49. Zheng, G., et al., *Hollow carbon nanofiber-encapsulated sulfur cathodes for high specific capacity rechargeable lithium batteries.* Nano letters, 2011. **11**(10): p. 4462-7.
50. Singh, D.P., et al., *Facile Micro Templating $LiFePO_4$ Electrodes for High Performance Li-Ion Batteries.* Advanced Energy Materials, 2013. **3**(5): p. 572-578.
51. Ren, X., et al., *Properties, preparation and application of black phosphorus/phosphorene for energy storage: a review.* Journal of Materials Science : Full Set - Includes `Journal of Materials Science Letters', 2017. **52**(17): p. 10364-10386.
52. Zhao, J., et al., *Phosphorene as a promising anchoring material for lithium-sulfur batteries: a computational study.* JOURNAL OF MATERIALS CHEMISTRY. A, 2016. **4**(16): p. 6124-6130.
53. Harks, P.P.R.M.L., F.M. Mulder, and P.H.L. Notten, *In situ methods for Li-ion battery research: A review of recent developments.* Journal of Power Sources, 2015. **288**: p. 92-105.
54. Liu, D.X., et al., *In Situ Quantification and Visualization of Lithium Transport with Neutrons.* Angewandte Chemie, 2014. **126**(36): p. 9652-9656.
55. Oudenhoven, J.F.M., et al., *In Situ Neutron Depth Profiling: A Powerful Method to Probe Lithium Transport in Micro-Batteries.* Advanced Materials, 2011. **23**(35): p. 4103-4106.